The effects of amino acid substitutions near the N-terminus on thermal adaptation of VPR, a subtilisin-like serine proteinase from a psychrotrophic *Vibrio*-species

Arnar Sigurðsson

Raunvísindadeild
Háskóli Íslands
2016

The effects of amino acid substitutions near the N-terminus on thermal adaptation of VPR, a subtilisin-like serine proteinase from a psychrotrophic *Vibrio*-species

Arnar Sigurðsson

15 ECTS thesis submitted in partial fulfillment of a
Baccalaureus Scientiarum degree in Biochemistry

Advisors
Magnús Már Kristjánsson, Professor
Co-advisors
Kristinn R. Óskarsson, Doctorate Student
Bjarni Ásgeirsson, Professor

Faculty of Physical Sciences
School of Engineering and Natural Sciences
University of Iceland
Reykjavík, 25.May.2016

The effects of amino acid substitutions near the N-terminus on thermal adaptation of VPR, a subtilisin-like serine proteinase from a psychrotrophic Vibrio-species
15 ECTS thesis submitted in partial fulfillment of a *Baccalaureus Scientiarum degree in Biochemistry*

Faculty of Physical Sciences
School of Engineering and Natural Sciences
University of Iceland
Hjarðarhagi 2-6
107, Reykjavík

Telephone: 525 4000

Bibliographic information:
Arnar Sigurðsson, 2016, The effects of site-directed mutagenesis near the N-terminus on thermal adaption of VPR, Bachelor‘s thesis, Faculty of Physical Sciences, University of Iceland, pp 40 .

Printing:
Reykjavík, Iceland, May 2016

Útdráttur

Rannsóknaverkefnið er byggt á fyrri rannsóknum sem unnar hafa verið á rannsóknarstofu leiðbeinanda og snúa þær að því að útskýra forsendur hitastigsaðlögunar og þá byggingalegu þætti sem stuðla að auknum hitastöðugleika í subtilisin-líkum serín próteinasa VPR, úr kuldakærri *Vibrio* tegund. Til þess að reyna að auka hitastöðugleika ensímsins voru gerðar samanburðarrannsóknir við ensímið aqualysin I (AQUI) úr hitakæru örverunni *Thermus aquaticus* sem hefur samsvarandi þrívíddarbyggingu og valdar út mögulegar stökkbreytingar fyrir VPR með AQUI sem módel til þess að auka hitastöðugleika VPR. Notað var C-enda stytta afbrigðið af VPR ($VPR_{\Delta C}$) við rannsóknina og tvær stökkbreytingar, önnur sem hefur áður verið gerð $VPR_{\Delta C}$_N3P/I5P, sem olli mikilli aukningu í stöðugleika gegn hitaafmyndun, en einnig miklu tapi í virkni. Hitt stökkbrigðið sem rannsakað var er $VPR_{\Delta C}$_W6Y. Sú stökkbreyting hafði áður verið rannsökuð og sýnt að hún olli minnkun í hitastöðugleika án þess að hafa mikil áhrif á virkni. Stökkbreytingarnar eru báðar nálægt N-enda próteinsins og þar er mikilvægt Ca^{2+} bindiset (Ca3) sem einnig er til staðar í AQUI. Tilgátan var sú að stökkbreytingarnar kunni að hafa áhrif á þetta bindiset og ætti $VPR_{\Delta C}$_N3P/I5P að hafa hærra kjörhitastig vegna aukins stöðugleika gagnvart hitafmyndun og gæti það verið merki um sterkari bindingu við Ca^{2+} jónir í þessu bindiseti en hjá $VPR_{\Delta C}$_W6Y, þar sem mikil lækkun var í stöðugleika og er tilgátan að kjörhitastig ætti að vera lægra fyrir þetta ensím og ætti það einnig að vera viðkvæmara fyrir hitaafmyndun vegna minnkaðrar bindisækni Ca3 bindisetsins.

Til að kanna áhrif þessara stökkbreytinga á hitastigsaðlögun ensímsins voru framkvæmdar mælingar á kjörhitastigi (T_{opt}) $VPR_{\Delta C}$, $VPR_{\Delta C}$_N3P/I5P og $VPR_{\Delta C}$_W6Y. Niðurstöður þeirra mælinga leiddu í ljós smávægilega lækkun í hitastigsaðlögun fyrir $VPR_{\Delta C}$_N3P/I5P sem er þó vart marktæk þar sem kjörhitastigsferlar $VPR_{\Delta C}$ og $VPR_{\Delta C}$_N3P/I5P voru nánast óaðgreinanlegir og lækkunin var innan við 1 °C. Hins vegar var skýr breyting í $VPR_{\Delta C}$_W6Y þar sem kjörhitastig lækkaði um 7-8 °C. Til að skýra það betur voru gerðar hitaafmyndunar-tilraunir ($T_{50\%}$) á $VPR_{\Delta C}$_W6Y og $VPR_{\Delta C}$ og borinn saman hitastöðugleiki þeirra yfir bilið 0 – 30 mM af $CaCl_2$ til að rannsaka stöðugleika ensímanna gagnvart $CaCl_2$ styrk.

Niðurstöður leiddu í ljós að VPR_{Δ}_W6Y hefur minni bindisækni í Ca^{2+} jónir heldur en $VPR_{\Delta C}$, við 1mM EDTA við 0 og 1 mM styrk af $CaCl_2$ er lítil sem engin stöðugleika aukning í stökkbrigðinu í samanburði við $VPR_{\Delta C}$. Hitastöðugleiki beggja ensímanna byggist á Ca^{2+} styrk í lausninni en gífurlega mikill munur er á milli $VPR_{\Delta C}$ og $VPR_{\Delta C}$_W6Y, þar sem stökkbrigðið er mjög óstöðugt gagnvart hitaafmyndun.

Abstract

The research project is based upon previous studies that have been done at the lab of the instructor and their aim was to study the structural properties involved in temperature adaptation of a subtilisin-like serine protease VPR, from a psychrophilic *Vibrio* species. In order to increase the thermal stability of the enzyme, mutations were selected on the basis of comparisons to a homologous thermophilic enzyme, aqualysin I, from the thermophilic bacterium *Thermus* aquaticus. For this study, a truncated form of VPR was used ($VPR_{\Delta C}$) with a shortened C-terminus. Two different mutations were done on the $VPR_{\Delta C}$ gene, a previously studied $VPR_{\Delta C}$_N3P/I5P which resulted in increased thermal stability of the protease, but which also decreased its catalytic efficiency significantly. The second variant, $VPR_{\Delta C}$_W6Y led to a decrease in thermal stability with no significant change in k_{cat}. Both substitutions are located at the N-terminus and also close to a calcium binding site (Ca3) which is also present in AQUI.

The hypothesis is that these substitutions may affect the Ca3 binding site and cause a change in the thermal adaptation of the enzyme. To test this hypothesis we theorized that $VPR_{\Delta C}$_N3P/I5P should have a higher optimal temperature (T_{opt}) than $VPR_{\Delta C}$ due to its increased stability against thermal denaturation. $VPR_{\Delta C}$_W6Y has shown a significant decrease in its stability against thermal denaturation ($T_{50\%}$) and we estimated that it would shift its T_{opt} towards colder temperatures than that of $VPR_{\Delta C}$ due to the placement of the altered residue and that its lower stability against thermal denaturation is due to lowered affinity for Ca^{2+}-binding.

The results of optimal temperature assays showed no significant change in T_{opt} for $VPR_{\Delta C}$_N3P/I5P, the change was within 1 °C and can be estimated as operator error. $VPR_{\Delta C}$_W6Y, however, showed a decrease of 7-8 °C in optimal temperature and supported the hypothesis that the mutation had shifted the temperature optimum of the enzyme. To study the effects of the mutation further $T_{50\%}$ assays were performed on $VPR_{\Delta C}$_W6Y and $VPR_{\Delta C}$ for comparison. The enzymes were assayed against 0 – 30 mM concentrations of $CaCl_2$ to determine the effects of calcium concentrations on their stability. Results showed that $VPR_{\Delta c}$_W6Y may have less affinity for Ca^{2+} ions than $VPR_{\Delta C}$, the strongest evidence for this is seen in the 0 – 1 mM concentration comparison for $VPR_{\Delta C}$ and $VPR_{\Delta c}$_W6Y where $VPR_{\Delta C}$ showed an increase in stability between those two data points, whereas VPR_{Δ}_W6Y did not. It is most likely a result of lowered affinity for Ca^{2+} whereas the enzyme is not able to compete for calcium ions with 1mM EDTA at 0 and 1 mM concentrations of $CaCl_2$. The stability of both enzymes was increased with increased $CaCl_2$ concentrations but there was a significant difference in thermal stability between $VPR_{\Delta C}$ and $VPR_{\Delta C}$_W6Y, where $VPR_{\Delta C}$_W6Y was much more sensitive to thermal denaturation than $VPR_{\Delta C}$.

Table of contents

List of Figures

List of Tables

Acknowledgements

I would like to thank Magnús M. Krisjánsson, the instructor of this project for his guidance during this project. I also want to thank Kristinn Ragnar Óskarsson the co-instructor for his help in the laboratory and with other work related to this project and Jens G. Hjörleifsson for interesting conversations and help and Bjarni Ásgeirsson as well and my fellow students Arnór Freyr Sævarsson and Étienne Leon Poisson for the past 3 years of university studies together. And last but not least I would like to thank the Faculty of the Science Institute of Iceland and the teachers of the Univeristy of Iceland.

1 Introduction

Subtilisin-like serine proteases are a highly diverse group of enzymes found across all domains of life and are used in various industrial processes with the main focus being in detergents due to their alkaline activity optima and ability to function at high temperatures. Therefore, research focusing on increasing their thermal stability and activity under high temperature, chelating and oxidizing conditions has received much attention [1].

Many methods can be utilized to achieve directed evolution towards increased stability, activity, or resistance to oxidizers. Research groups often use non-specific methods such as error-prone PCR and saturation mutagenesis to create gene libraries of beneficial mutations [2], Then after the selection is carried out for the desired property of variants and their mutations can then further be recombined with other selected mutations to further improve the stability of their protein [3]. These methods are often useful although they are lacking the ability to be precisely controlled and it is time-consuming to test each of the new variants from the tests [4].

This thesis is involved with research being done at the lab of the main instructor Magnús Már Kristjánsson and are focused on structural properties of thermal adaptation among subtilisin-like serine proteinases. The main subject of these research projects has been a subtilisin-like serine proteinase from a psychrophilic *Vibrio* species (VPR). The crystal structure of VPR has been determined, the structure was solved by means of molecular replacement and refined at 1.84 Å. The three-dimensional structure of the cold-adapted subtilase is homologous to enzymes of meso- and thermophilic origins, proteinase K and thermitase [5]. To study the properties of thermal adaptation, multiple mutations have been performed on VPR [8]. The mutations have been selected by comparing the structure of VPR to that of a thermophilic homologous enzyme, aqualysin I (AQUI). Such experiments have included incorporation of a new iron pair, deemed to be present in AQUI, into the structure of VPR, resulting in a ~3 °C increase in both $T_{50\%}$ and T_m [34]. Other experiments have substituted selected Xaa/Pro and Ser/Ala mutations into VPR, which were chosen based on comparison with AQUI and proteinase K, and led to increased thermal stability, but at the cost of catalytic efficiency [6,7]. Mutations located near the N-terminus of VPR have been most successful in improving thermal stability and activity on VPR, the mutation VPRΔC_N3P/I5P improved $T_{50\%}$ by 5.7-5.9 °C but resulted in an eightfold decrease in k_{cat} for the enzyme [8]. Another mutation, Trp6Tyr (VPR_W6Y), caused a decrease in $T_{50\%}$ by 11-12 °C without any substantial change in activity [9]. These two mutations are the main subject of this thesis.

1.1 Temperature adaptation

Throughout evolution, bacteria have become able to occupy almost every niche on the planet and their cellular component and machinery have had to keep up with environmental changes. To achieve this, life has developed many different ways to maintain protein stability and function, although it is clear that proteins are very complex structures and there is no one correct route proteins take to maintain their structure and function during evolution. *Figure 1* describes the relationship between thermostability and catalytic activity at low temperatures homologous enzymes, the pink area represents naturally occurring enzymes with minimal stability and activity that are required for biological function, and the blue shaded are is for enzymes that have high thermal stability and activity at low temperatures. The white area in the upper right corner would be both highly thermostable proteins that would also be highly active at low temperatures. Laboratory experiments have seen this adaption for enzymes since it is accessible through evolution but not biologically relevant [10].

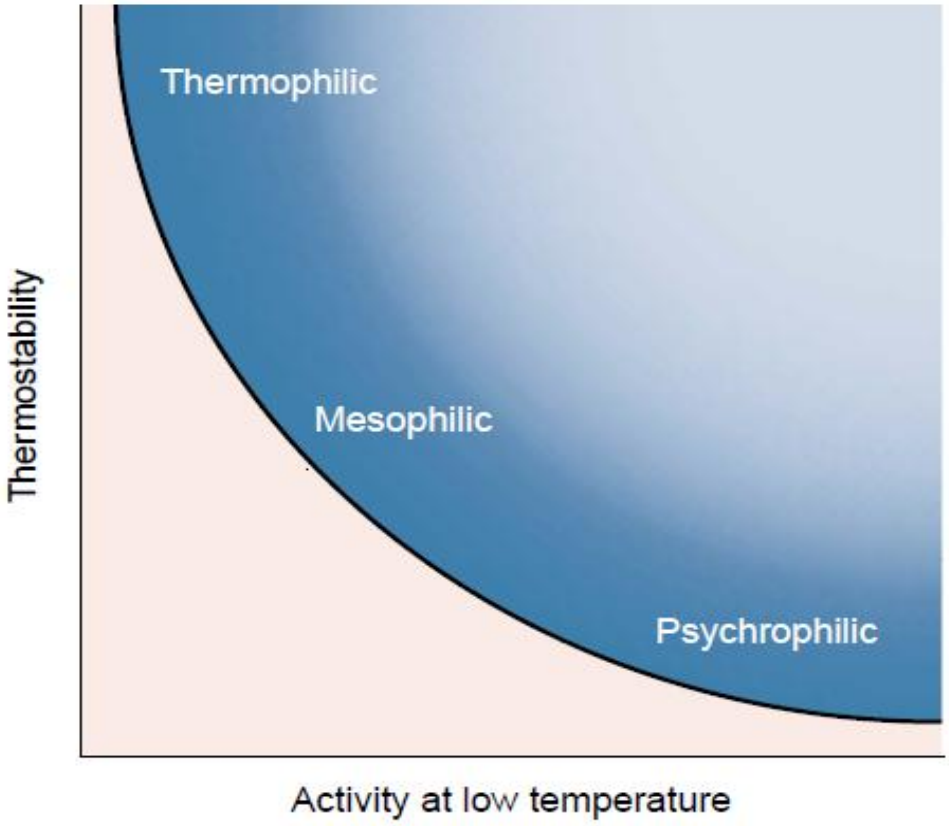

Figure 1. The relationship of catalytic activity and structural stability: *For homologous enzymes adapted to different temperatures there is shown a trade-off between activity at low temperatures and thermostability. This is a result of the interactions between structural properties and catalytic properties of the enzyme, a more rigid structure can provide increased stability against thermal denaturation but at the cost of catalytic efficiency [10].*

Thermophilic adaptation is a result of enforcement in stabilizing properties of non-covalent interactions such as hydrophobicity, hydrogen bonds, salt bridges and van der Waals interactions, which may lead to more rigid structures, better suited for function at high temperatures. Psychrophilic life-forms, on the other hand, might reduce the number of stabilizing interactions in order to be able to operate at low temperature and mesophiles are somewhere in between. Therefore, in the case of a thermophile, it might use a stronger hydrophobic core, a mesh of salt bridges or increased number or stronger hydrogen bonds to increase the stability of its proteins. They also have other options including improving the binding of metal ions into their structure through specialized bindings sites, or by incorporating new sites. Depicted in *figure 2* is the conformational coordinate of psychrophiles and thermophiles against the free energy in a two-dimensional energy well as a folding funnel. The top of the funnel is a representation for the unfolded state of the enzymes and the bottom is the folded state, the height of the funnel correlates to the free energy of folding and conformational stability.

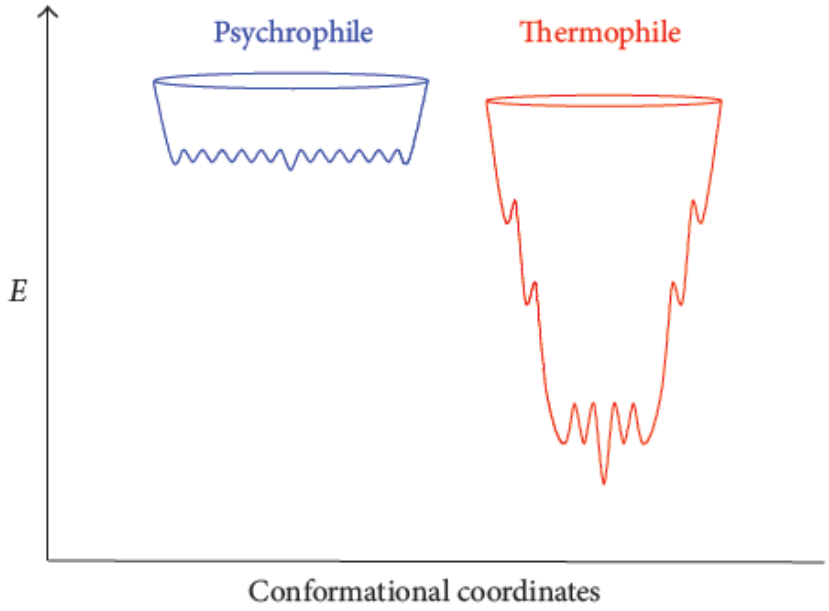

Figure 2. Properties of conformation in thermal adaption: Conformational coordinates of a psycrophile vs. a thermophile. The low conformational stability of psychrophiles is a result of few stabilizing factors to the protein structure. The protein structures can change their conformations and it gives the ability to operate at low temperatures. The thermophile needs to be in a very stable form with relatively low energy in its structure since it is in a very energy rich environment [12].

These stabilizing forces, however, are counterbalanced by entropy, which is also essential to maintain the function of enzymes since their catalytic activity is often dependent on their ability to change their conformations [11]. The area of the funnel at a given point can be considered as entropy or number of microscopic configurations within the system (eq. 3) The further down we go into the funnel, the smaller is the area of conformation, indicating an

increase in stability, but at the cost of lower internal energy. Thermophilic enzymes use stronger intramolecular forces to maintain their structures and rely on the heat from the environment to provide sufficient entropy to maintain their flexibility needed for their function [12]. Psychrophilic enzymes, on the other hand, need to be optimized for higher entropy at lower temperatures and have low structural stability. At low temperatures, water is more viscous which results in slower diffusion rates. Reduction in diffusion rates and the increased viscosity makes it harder to acquire resources and, therefore, cold-adapted enzymes with enhanced catalytic efficiency must be used. The flexibility of these enzymes is crucial to obtain high catalytic efficiency at low temperatures and they are able to do so through combination of several features, increasing the number of hydrophobic amino acids that are exposed to the solvent, a larger solvent accessible area, a less compact hydrophobic core, increased number of glycine and lysine residues and reducing the number or prolines and arginine residues, including reducing the numbers of hydrogen bonds and salt bridges in the enzyme [5, 13]. To better understand the biophysical properties of catalytic reactions and stability, we need to look at what factors are involved in the turnover rate.

$$k_{cat} = \kappa \frac{k_B \cdot T}{h} \cdot e^{-\frac{\Delta G^{\#}}{R \cdot T}} \qquad (Eq. 1)$$

$$\Delta H^{\#} = Ea - RT \qquad (Eq. 2)$$

$$\Delta S^{\#} = \frac{\Delta H^{\#} - \Delta G^{\#}}{T} \qquad (Eq. 3)$$

Equation 1 describes the turn-over rate k_{cat} as a function of temperature. In the equation, κ is the transmission coefficient generally assumed to be close to 1, k_B is the Boltzmann constant, h is the Planck constant, R is the universal gas constant and $\Delta G^{\#}$ is the free energy of activation [12]. Equation 2 describes the enthalpy of activation which is dependent on the activation energy (Ea) and the universal gas constant and temperature. Equation 3 describes the entropy of activation. The free energy of activation is dependent on the enthalpy of activation, which comes from the internal energy of the system that can arise from covalent and non-covalent interactions in the structure of the enzyme. The free energy is also dependent on the entropy of activation, or number of microscopic configurations within the system. Thermophilic enzymes tend to have a higher enthalpy of activation of unfolding which is connected to its rigid structure which increases the energy of activation, whereas psychrophiles would have increased entropy by lowering the energy of activation. Since microbes are unable to regulate internal temperature like mammals they have increased evolutionary pressure to select molecular mechanisms that are suitable for their environment, as previously stated for thermophiles, they require stability against thermal denaturation, they can do so by increasing their enthalpy of activation (Eq. 2), the only factor they can affect is the energy of activation [9, 10, 11, 14, 15].

1.2 Serine proteases

Serine proteases are enzymes that cleave peptide bonds using serine as the nucleophilic amino acid at its active site. Serine proteases are divided into 13 clans and 40 families [17]. Serine proteases such as subtilisin-like and chymotrypsin-like enzymes use a catalytic triad Asp-His-Ser in their catalytic mechanism. Aspartic acid is acidic and in the reaction center it stabilizes the charge on the histidine residue, which acts in the mechanism as a base catalyst, removing a proton from the side chain of the serine residue thus activating it as a nucleophile, attacking the carbonyl group of the peptide bond to be cleaved to form a tetrahedral intermediate, the reaction mechanism is shown in *figure 3*. The histidine residue has a positive charge on its side chain due to a proton which is removed by the cleavage of the peptide bond and is transferred to the cleaved product. An acyl-enzyme intermediate is formed which is then hydrolyzed as the histidine pulls a proton from an incoming water molecule which then becomes a nucleophile and attacks the acyl-enzyme intermediate, forming another tetrahedral intermediate, followed by the release of the second peptide product and liberation of active site serine residue finalizing the hydrolysis of the peptide bond. The serine residue then regains a proton by removing it from the histidine residue and then the enzyme is ready to cleave another bond [17,18].

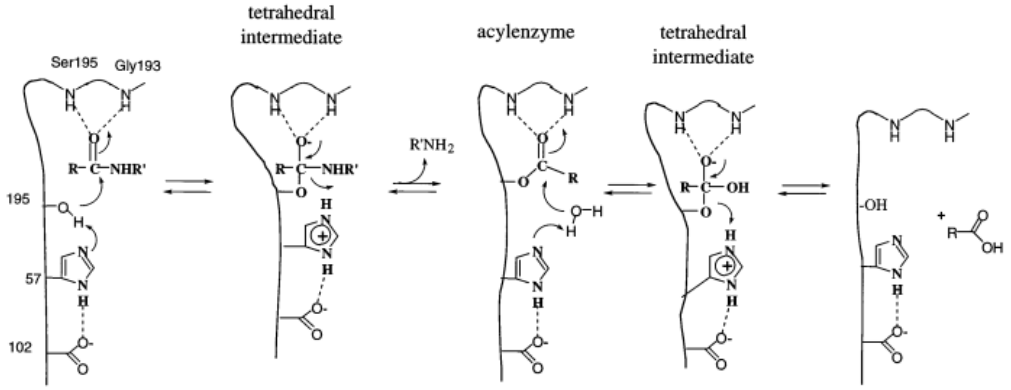

Figure 3. The catalytic mechanism of a serine protease. *The hydrolysis of peptide bonds by serine proteases is done by the catalytic triad of Asp, His, and Ser. Asp induces His, which in turn grabs a proton from Ser making a nucleophile able to make a tetrahedral intermediate with it's substrate. The substrate is catalyzed into an acyl-enzyme intermediate after cleaving the peptide bond, the product is released after a water molecule attacks the acyl compound and re-protonates the Ser residue [15].*

In the Merops database, proteases are classified based on hierarchical, structure-based classification. Where each peptidase is assigned to a family on the basis of the statistical significance of similarities in the amino acid sequence and families that are thought to be homologous are assigned to a clan [21]. The largest clan of serine proteinases is the PA clan, containing 13 families using the catalytic triad order of His-Asp-Ser and primary specificity for A, E, F, G, K, Q, R, W and Y. The clan is represented by the trypsin fold and is probably one of the best-studied clan of serine proteinases. Most PA clan proteinases have

trypsin/chymotrypsin-like substrate specificity and have either high affinity for the positive side chains of arginine and lysine, at the P1 position of the substrate for trypsin-like, but large hydrophobic residues like phenylalanine (F) tryptophan (W) or tyrosine (Y) for chymotrypsin-like proteases. In *figure 4*, the catalytic triad of chymotrypsin is shown. The Asp102 acts on His57 which activates the nucleophilic properties of the Ser195 side chain [14]. The proteases of PA clan have diverse functions and are mediators in key biological processes such as digestion, blood coagulation, and immune response, where the protease domain is connected to one or more regulatory domains such as EGF, fibronectin, kringle, or von Willebrand factor domains [19].

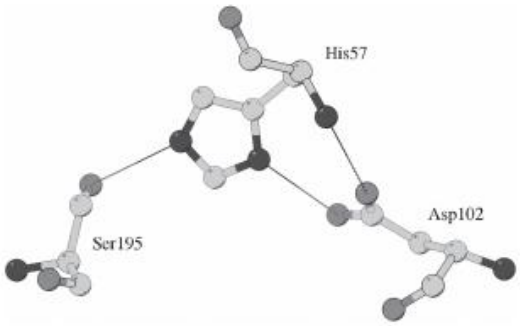

Figure 4. The catalytic triad of the SB clan. The order of the catalytic triad is Asp, His, Ser, the lines represent the interactions between the residues in the form of hydrogen bonds (PDB ID: 4CHA) [14].

The SB clan, to which VPR belongs to, is quite smaller with only two families [16]. Similarly, to the PA clan the SB clan uses the catalytic triad but in a slightly different order, i.e. Asp-His-Ser and have primary specificity for F, W, Y. The order of the amino acids in the catalytic triad does not matter as long as they are close enough to each other to interact in the reaction center. The representative member of the SB clan is subtilisin [19]. The SB clan is divided into the S8 family and S53 family, where S8 is then divided into two subfamilies S8A and S8B. The S8A family is represented by subtilisin and S8B is represented by kexin. Both families are essential for protein processing to obtain nutrition and tend to hydrolyze peptide bonds at the C-side of large hydrophobic residues [20].

1.2.1 Subtilisin-like serine proteases

Subtilases (S8A) are a diverse group of serine proteases that are most often produced as multi-domain proteins with a α/β structure composed mainly of parallel β sheets arranged in βαβ units. The fold is characterized by a three layer αβα sandwich with a parallel β sheet of seven strands sandwiched between the α helices. The topology is called a Rossmann fold. In VPR, the cold-adapted enzyme, the α helices surround the β sheet and are connected to the strands by loops that lie on the surface. As seen in *figure 5*, the enzyme makes use of long loops to achieve conformational flexibility [9, 11]. Subtilases usually have three stages during maturation, the first being a preproenzyme where it has a signal peptide for secretion across a membrane and a prodomain which is essential for correct protein folding. The prodomain is, therefore, referred to as an intramolecular chaperone (IMC) [1]. After secretion and IMC mediated protein folding, the protein undergoes autoproteolytic cleavage of the covalent link between the IMC domain and the enzyme resulting in a mature enzyme as depicted in *figure 7* [1].

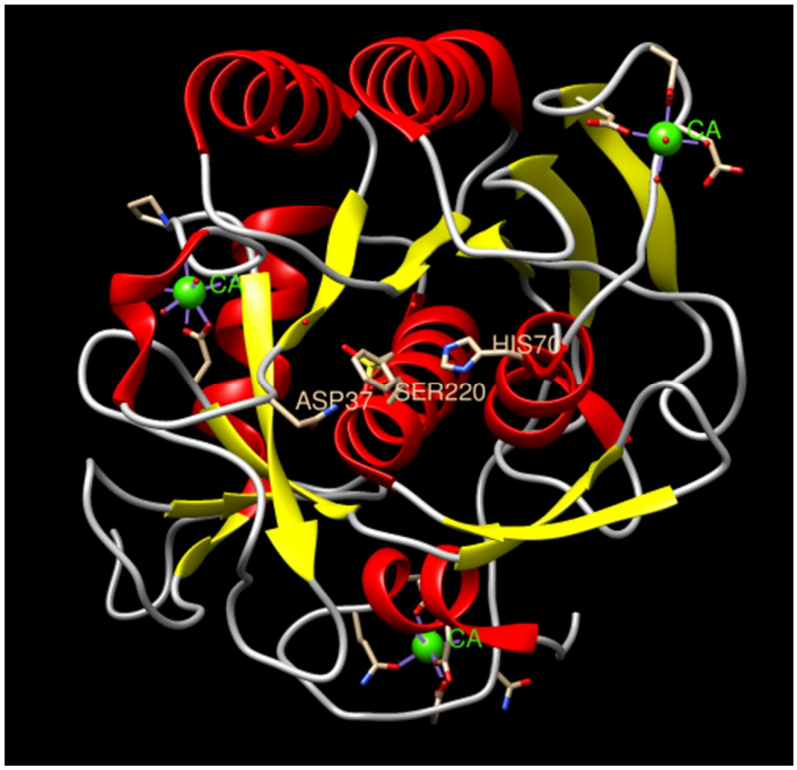

Figure 5. The crystal structure of VPR T 1.84 Å resolution. In the reaction center residues of the catalytic triad are marked by annotations and the serine residue is complexed with PMS inhibitor. The secondary structure is colored in red (helices), yellow (beta-strands) and gray (loops). Calcium ions are colored green, the calcium site on the left is Ca1, upper right is Ca2 and at the bottom of the figure is binding site Ca3 (PDB ID: 1SH7) [5].

In the folding process of subtilisins, the prodomain is able to catalyze the folding even as a separate polypeptide chain [22, 23]. During the folding process, the prodomain acts as a competitive inhibitor of the protein complex and when the enzyme has matured it autocatalytically cleaves the prodomain [23]. Prodomain-assisted folding is common in extracellular proteases, including subtilisins and chymotrypsin-like enzymes [24].

Many subtilases have calcium binding sites which are important for function and structural stability. Therefore, it is important that experiments using subtilases are carried out to account for the effects with respect to calcium concentrations. Folding of subtilisins is aided by calcium binding late in the folding process. The protein undergoes an intermediate state between the unfolded and folded states where the prodomain is bound and then reaches a native state, but the native state is stabilized by calcium binding. The number of calcium binding sites differ from enzyme to enzyme but overall very few contain no calcium binding sites. The calcium sites form a high energy barrier that provides kinetically and thermal stability of the enzyme. Experiments that have used high amounts of EDTA or point mutations to remove calcium from their binding sites have shown reduced stability of the protein against thermal denaturation [1, 25, 40].

1.2.2 VPR a psychrotrophic subtilisin-like serine protease

VPR is a psychrophilic subtilisin-like serine protease found in a psychrotrophic *Vibrio* species (strain PA-44). The enzyme is secreted as a 47-kDa protein and autoproteolytic catalysis at the N-terminus results in a 36 kDa and final maturation is the cleaving of the prodomain of the C-terminus which results in a fully mature protease that is approximately 28 kDa as seen in *figure 7*. The synthetic substrate succinyl-AAPF-*p*-nitroanilide has been used to study properties of the protein [26]. The topology of VPR as shown in *figure 7*, consists of a β sheet made from 7 parallel strands and 2 antiparallel strands with a switch point between strands 1 and 4 where the active site is, there are six α helices and one 3/10 helix labeled γ on *figure 6* [5].

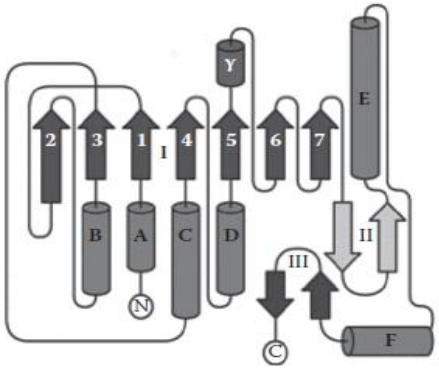

Figure 6. Topological diagram of the VPR structure [1].

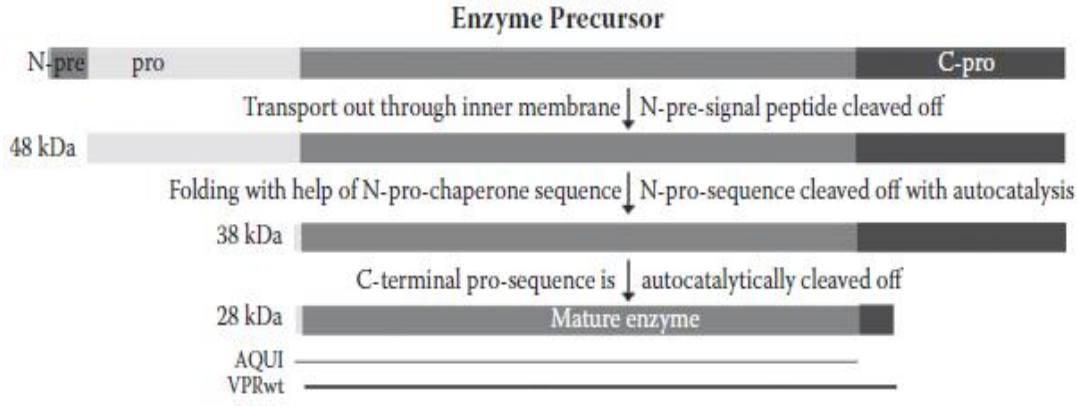

Figure 7. Stages of maturation for VPR and AQUI: *Maturation stages of AQUI and VPR_{wt}, Both are very well characterized subtilases. In the figure are shown three steps of maturation for the enzymes. The strands annotated with AQUI and VPR_{wt} are shown in different colors and at different positions of the enzyme precursor schematic, that is to infer that the N-terminus on AQUI is slightly longer than that of VPR_{wt} and shorter at the C-terminus.[1]*

The structure of VPR is a Rossmann fold with three calcium binding sites which are very important for protein stability and final stages of folding. Tthe three-dimensional structure of VPR is shown in *figure 5* where the catalytic triad is annotated (Asp37-His70-Ser220) and calcium is shown in green and the residues that are involved in calcium binding are shown as well. There are three disulfide bridges that are not shown in *figure 5*, Cys67-Cys99, Cys163-Cys194, and Cys277-Cys281. In *figure 5* the substrate binding pocket is not annotated, it is located in a cleft lined by residues 100-103 on one side and 130-133 on the other. The S1 substrate binding pocket is made up of the residues A154-A155-G156 [5]. When comparing the structure of VPR to the structures of thermitase and proteinase K, it was observed that the enzyme contained an additional Ca binding site (Ca-3 that had not been seen previously in the structures of other characterized subtilisin-like proteases. The first calcium binding site (Ca1) in VPR (seen in *figure 8*) is analogous to the Ca1 site in proteinase K, the calcium is coordinated by Oδ1 and Oδ2 of Asp196, the carbonyl oxygen of Pro171 and Gly173 and two water molecules. This binding site is well conserved among members of the proteinase K family. A second binding site (Ca2) is also seen in thermitase and described as a medium-strong binding site [5]. The calcium ion is stabilized by interactions with Oδ1 and Oδ2 of Asp61, Oδ1 and Oδ2 of Asp 63 and interacts with three water molecules that coordinate the calcium ion. From sequence analysis of related proteins, this binding site should be highly homologous to the proteinases from *Vibrio alginolyticus* and *Vibrio cholerae*, but is absent in thermophilic proteinases from *Thermus* Rt41a and AQUI from *Thermus aquaticus.* Calcium binding sites 1 and 2 are comparable to that of Subtilisin which has a K_a of 10^7 M^{-1} and 6.7 x 10^4 M^{-1} respectively, at 25 °C. Where calcium binding site 1 of VPR is similar to that of the weaker calcium binding site in subtilisin [1]. The third calcium-binding site, which was first

described in VPR is situated close to the N-terminus. The calcium ion is linked to an α helix and the residues of the succeeding surface loop and is coordinated by the side chain and carbonyl oxygen of Asp9, Asp12, Gln13, Asp19, the carbonyl oxygen of Asn21 and 1 water molecule [5].

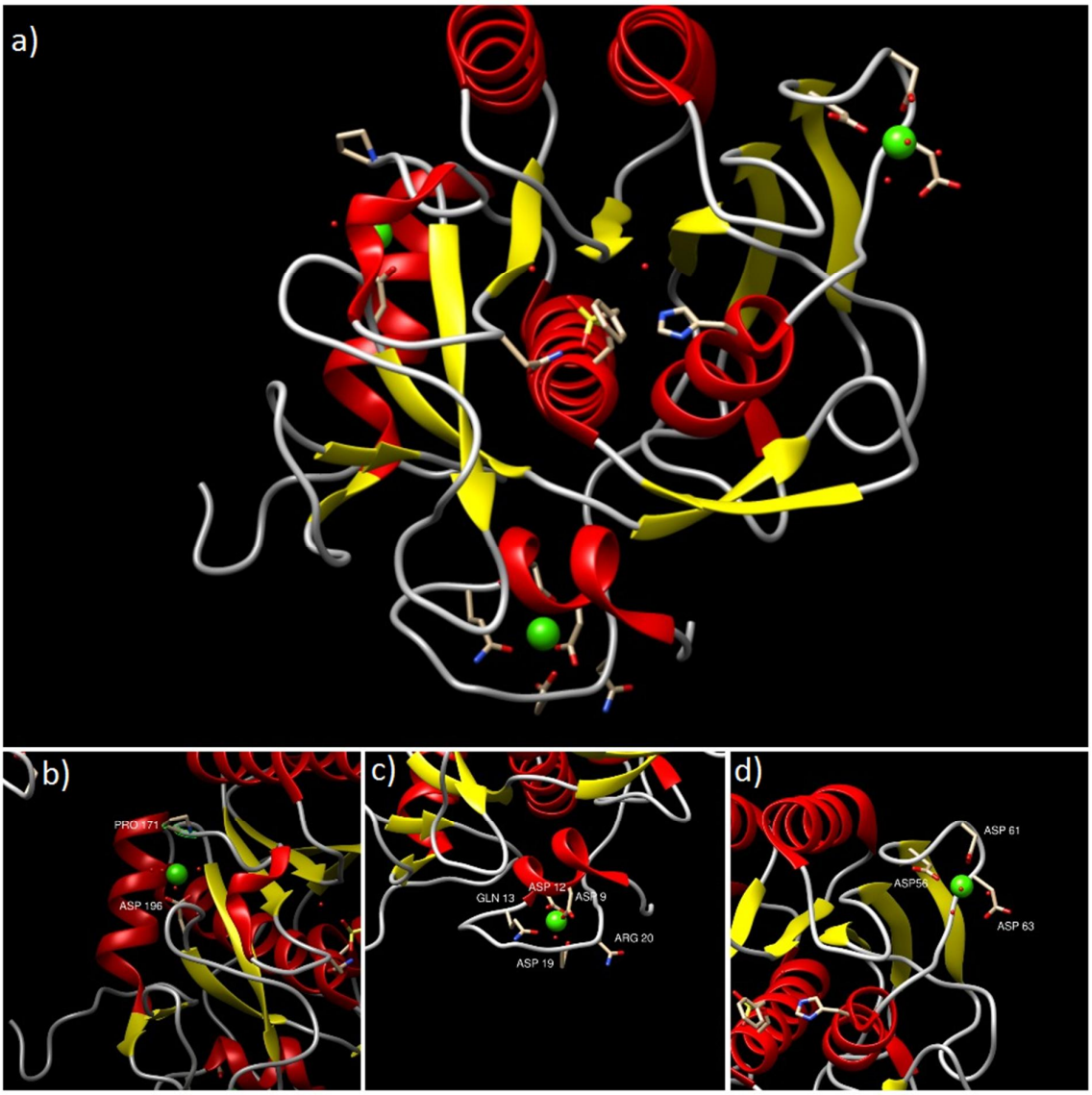

Figure 8. The calcium binding site of VPR: *a) The three-dimensional structure of VPR. b) Ca1 binding site, the interacting residues are Asp196, Pro171, and Gly173. C) Ca3 binding site, the interacting residues are Asp9, Asp12, Gln13, Asp19 and Arg 20. d) Ca2 binding site, the interacting residues are Asp 56, Asp61 and Asp63. Water molecules are not shown in this figure (PDB ID: 1SH7) [5].*

1.3 Rational design of improved heat tolerance and activity

The stability of a protein's native state is affected by many factors, heat, pressure, pH, ion concentration, or proteolysis. From a physical perspective, the stability is reliant on both thermodynamic and kinetic factors. Thermodynamic stability of the protein is governed by the energy in the open system, as in the states of equilibrium (number of conformations or molecular rotations/vibrations) and free energy barriers between folding states. For thermophiles kinetic and thermodynamic stability is very important, but in psychrophiles, thermodynamic stability is reduced in order to maintain the ability to change its conformation but it is also important to acknowledge that there is very little evolutionary pressure for increased thermal stability in psychrophiles [8].

Comparative studies of structures of homologous enzymes have been used for selecting specific mutations selected for the purpose of altering enzyme properties (rational design), Such comparisons have been carried out for VPR and AQUI as models for explaining the difference in thermal stability of the enzymes, an overlap of the VPR and AQUI structure is shown in *figure 9* to illustrate the homology of the fold between the enzymes [8].

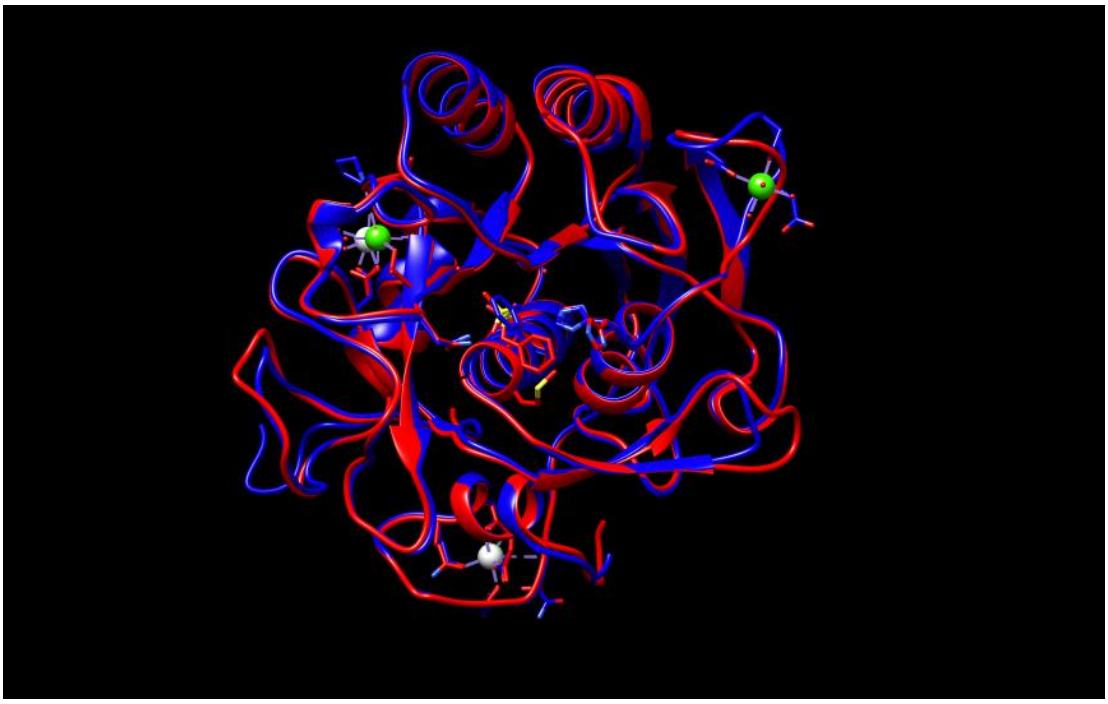

Figure 9. An overlap of the structure of VPR (blue, calcium green) PDB ID: 1SH7 and AQUI (red, calcium white) PDB ID: 4DZT. The structures are nearly identical in folding and catalyze the same substrate (sAAPF-p-NA). VPR is psychrotrophic and AQUI 1 is thermophilic, thus, by comparing the structures and selecting amino acid sequences that are able to increase hydrogen bonds, salt bridges or disulfide bridges may result in increased thermal stability [8].

Many strategies have been used for the rational design of enzymes with different results. Some of the approaches used included salt bridge optimization [6, 26], substituting proline

into the sequence to increase rigidity in the protein [7], stabilizing α-helixes [27], incorporating new disulfide bonds to increase intramolecular forces [28], cavity filling to decrease access of water to the protein, stabilizing the protein core [24] and even replacing polar residues inside the protein or on its surface [30,31].

A C-terminal truncated form of VPR was previously made for comparative studies since the C-terminus of VPR is longer than that of AQUI (*figure 7*) [32]. Former experiments on VPR aimed at increasing thermal stability have been most successful by incorporating amino acid exchanges near the N-terminus of the enzyme. Previous experiments on VPR have been carried to incorporate new ion pairs into the structure of VPR (wt and ΔC). Two mutations were tested for, the VPR_{wt} _N15D and N15D/K257R. The N15D mutation resulted in an increase in $T_{50\%}$ of about 2.8 °C and an increase of 2.7 °C in T_m for the wild-type enzyme. The mutation N15D/K257R however only showed an increase of about 0.2 °C in $T_{50\%}$ and 1.5 °C in T_m. Only the N15D mutation was tested for $VPR_{\Delta C}$, it increased the $T_{50\%}$ value by 3.2 °C. All mutations showed an increase in catalytic efficiency for VPR_{wt} but reduced the catalytic efficiency in variants of $VPR_{\Delta C}$ [6]. The structural effects of proline substitutions on VPR_{wt} I5P and N3P/I5P have also been tested. The mutations were done on the truncated form $VPR_{\Delta C}$. The insertion of the single proline (I5P) increased $T_{50\%}$ by 2.3 °C and T_m by 2.4 °C with a decrease in catalytic efficiency of about 147 units. In the double variant N3P/I5P $T_{50\%}$ was increased by 5.5 °C and T_m by 4.1 °C, but most notably the catalytic efficiency dropped dramatically, from 371 $mM^{-1}s^{-1}$ to 40 $mM^{-1}s^{-1}$ [34].

1.4 Aim of the project

This project is involved with ongoing research at the lab of the instructor and is focused on the structural properties of thermal adaptation among subtilisin-like serine proteases. The focus is on rational design of improved thermostability and activity. The goal is to select mutations from aqualysin I (AQUI) to implement stabilizing changes into VPR. The mutations that have been most successful are located close to the N-terminus of the VPR protease in close proximity to the Ca-3 binding site. The selected mutations to be studied here are $VPR_{\Delta C}$_N3P/I5P which increased thermostability by 5.5 °C but resulted in an eight-fold decrease in k_{cat} for the enzyme [34], and VPR_W6Y, that caused a reduction in $T_{50\%}$ by 11-12 °C without significant decrease in k_{cat} at 25 °C (Kristjánsson M.M. unpublished data).

From the observed data from prior studies, the increase in thermal stability and effects on the catalytic efficiency of the enzymes could indicate a shift in optimal temperature for the activity of the enzymes. For the $VPR_{\Delta C}$_N3P/I5P variant, the increased thermostability of the enzyme and the lowered k_{cat} value might suggest that the enzyme structure would have become more rigid, and would require a higher temperature to obtain the same molecular flexibility for the activity of the wild-type enzyme at the usual assay temperature. It is, therefore, probable that the optimal temperature (T_{opt}) for activity may have shifted to higher temperatures. For the $VPR_{\Delta C}$_W6Y variant which had no significant change in k_{cat} but lowered $T_{50\%}$, it may be that the optimal temperature would be shifted to lower temperatures than that of $VPR_{\Delta C}$. The locations of the mutations are close to the Ca3 binding site, therefore, it is probable that the mutation might affect the binding affinity $VPR_{\Delta C}$ has for calcium ions. The lowered thermal stability of $VPR_{\Delta C}$_W6Y might be a result of lowered affinity for calcium ions at the Ca3 binding site. This was tested by performing $T_{50\%}$ assays over a range of 0 - 30 mM $CaCl_2$ concentrations and determining the rate of thermal inactivation.

2 Materials and methods

Molecular graphics and structural analyses were performed with the UCSF Chimera package. Chimera is developed by the Resource for Biocomputing, Visualization, and Informatics at the University of California, San Francisco (supported by NIGMS P41-GM103311) [39].

2.1 Production of variants

The production of the variants was carried out as described in references 8 and 34.

2.2 Protein purification

2.2.1 Purification of $VPR_{\Delta C}$_N3P/I5P

The purification of $VPR_{\Delta C}$_N3P/I5P was performed as previously described in reference 26. Pellets of cells containing the VPR variant were suspended in 50 mL of a buffer containing 25 mM Trizma (Sigma), 10 mM calcium chloride (Sigma), pH 8 (Buffer A). Then, 1 mL of lysozyme (50 mg/mL) (Sigma) and 10 µl DNAase (5 mg/mL) (Sigma) were added and the mixture was shaken gently for 2 hours before rapid freezing in liquid nitrogen and was then thawed at 4°C overnight while being shaken. The morning after the mixture was frozen again in liquid nitrogen and thawed at room temperature while being shaken and the same process repeated. The sample was then heated in a water bath at 40 °C for 1 hour to obtain the fully active and mature protease [8].

The cell lysate was then centrifuged at 20,000 x g and 4 °C for 45 minutes. The supernatant from the centrifugation was collected and ammonium sulfate (Sigma) ($(NH_4))_2SO_4$) was added to give 80 % (w/v) saturation. Then, the supernatant was centrifuged as previously described. The precipitate was collected and dissolved in 50 mL buffer A and stored at 4 °C overnight.

The sample was loaded (2 mL/min) onto a Z-D-Phe-TETA-Sepharose (N-carbobenzoxy-D-phenylalanyl-triethylenetetramine-Sepharose) column that had been equilibrated with buffer A using a BioLogic LP Low-Pressure Liquid chromatography system with a high-flow pump with a gradient mixer from BioRad and equipped with a UV and conductivity detectors. After sample loading, non-binding proteins and various molecules were eluted from the column with buffer A containing 0.5 M NaCl (Sigma). The column was then equilibrated again using buffer A and finally the VPR proteinase was eluted from the column using buffer A containing 2 M guanidinium chloride (Sigma) and collected in 2 mL fractions into sample

tubes containing 2 mL buffer A with added 3 M ammonium sulfate resulting in a total volume of 4 mL using a Model 2110 fraction collector from BioRad.

The fraction from the Z-D-Phe-TETA column was collected if the activity in fractions was greater than 0.1 U/mL. Pooled fractions were then loaded onto a phenyl-Sepharose column to concentrate the product. The phenyl-Sepharose column had been equilibrated with Buffer A containing 1 M ammonium sulfate. The column was then eluted by lowering the concentration of ammonium sulfate to 0.1 M by a linear gradient, this step removes further impurities and finally the protease was eluted using buffer A that contains 50% ethylene glycol by volume. The protease was then diluted to 25 % ethylene glycol with buffer A, frozen in liquid nitrogen and stored in a freezer at – 25 °C.

2.2.2 Zaman-Verwilghen protein quantitation

For protein quantitation of $VPR_{\Delta C}$_N3P/I5P, the Bradford method using the Coomassie Brilliant Blue G250 staining assay was performed, using the Zaman-Verwilghen variation [35]. The protein samples from different steps during purification were incubated at room temperature for 15 minutes prior to measurement in test tubes, the mix was 0.25 mL protein sample added to 2.75 mL of the Coomassie Blue solution. Absorbance measurements were carried out at 620 nm on a Cary 50 Bio UV - Visible spectrophotometer (Varian).

2.2.3 SDS-polyacrylamide gel electrophoresis (SDS-PAGE)

SDS-PAGE was performed to estimate protein purity of the final product. The gel electrophoresis was a Laemmli discontinuous system [36], the gel was comprised of two parts a stacking gel and a separation gel. The separation gel was made by mixing 6 mL of 30 % acrylamide/bis-acrylamide (Sigma), 3.75 mL of 1.5 M Tris-Cl pH 8.8, 150 µl of 20 % SDS, 5.03 mL of dH_2O and 15 µl of tetramethylethylenediamine (TEMED). The mixture was degassed. Finally, 75 µl of 10 % ammonium persulfate (APS) were added to initialize the polymerization of the acrylamide and the solution was transferred into the gel cast. The stacking gel was made by mixing 1.98 mL of 30 % acrylamide/bis-acrylamide, 0.5 mL of 0.5 M Tris-Cl pH 6.8, 150 µl of 20 % SDS, 9 mL of dH_2O and 30 µl of TEMED. The mixture was degassed and then 75 µl of 10 % APS was added to the mixture. The mixture was added to the top of the separation gels and protein samples prepared while the gel polymerized. A 10 well comb was used to make the wells in the stacking gel.

Protein samples were prepared by inhibiting them at 1 mM PMSF of final concentration, then 65 µl of the protein sample was transferred to an Eppendorf tube, 25 µl of NuPAGE – LDS sample buffer (was heated at 70 °C for 15 minutes for easier handling) and 10 µl of dithiothreitol were added to the tube. The mixture was boiled for 5 minutes prior to loading

the wells. Into each well 10 µl of the sample were used and 8 µl of the ladder PageRuler™ Prestained Protein Ladder 10-180 kDa from Thermo Scientific (Product #26616). The electrophoresis was carried out in buffer F. The stock of buffer F contained 0.25 M Tris pH 8.75, 1.9 M glycine, 10 mM EDTA and 0.5 % SDS, prior to use, the stock was diluted 5-fold with water which is the correct concentration for electrophoresis. After electrophoresis the gel was fixed using 50 % ethanol (v/v), 2 % phosphoric acid (v/v), washed 2x 20 minutes in H_2O and stained overnight with "Blue Silver" Coomassie staining solution, containing 10% phosphoric acid (v/v), 100 g/L ammonium sulfate, 1.2 g/L Coomassie Blue G-250 and 20% methanol (v/v) this is the classical Neuhoff dye recipe [37]. The gel was washed with H_2O and stored a 4 °C until further use.

2.3 Enzymatic assays

The activity of $VPR_{\Delta C}$, $VPR_{\Delta C}$_N3P/I5P, and $VPR_{\Delta C}$_W6Y was measured using the substrate, succinyl-AlaAlaProPe-p-nitroanilide, or sAAPF-p-NA (Bachem). The substrate was kept as a stock of 25 mM sAAPF-p-NA in DMSO and stored at 4 °C prior to use. General assays were carried out at room temperature using 0.5 mM sAAPF-p-NA in 100 mM Tris-Cl, 10 mM $CaCl_2$ and pH 8.6. The absorbance was measured at 410 nm over 30 seconds. The product of the enzyme catalysis has a molar attenuation coefficient of 8480 M^{-1} cm^{-1} which is used to determine enzymatic activity.

Equations 4 and 5 describe the calculational method used to calculate the velocity of catalytic reaction for the enzyme (Eq. 4) and by rewriting the equation we can solve for activity per milliliter (Eq. 5).

$$V = \frac{\Delta A/sec}{8480\ M^{-1}cm^{-1}} \cdot \frac{1000\ mM}{M} \quad \text{(Eq. 4)}$$

$$\frac{U}{mL} = \left(\frac{\frac{\Delta A}{min}}{8480 M^{-1}cm^{-1}} \cdot \frac{total\ volume}{volume\ enzyme} \cdot 1\ \mu mol \cdot 1\ cm \right) \cdot 1000 \frac{mL}{L} \quad \text{(Eq. 5)}$$

2.4 Optimal temperature (T_{opt})

For determination of optimal temperature (T_{opt}) of $VPR_{\Delta C}$ and its variants, measurements were done with a Heλios α UV-Visible spectrometer from Thermo Electron equipped with a Thermo Spectronic single cell Peltier system and using a quartz cuvette. Enzymes were diluted to an approximate activity of 1 U/mL and assayed using 0.5 mM sAAPF-p-NA diluted in 100 mM Tris-Cl, 10 mM $CaCl_2$ at pH 8.0. The assay buffer was adjusted to appropriate pH for the temperature of the measurement, Tris-Cl changes in pH with temperature by the relationship $\Delta pH/°C = -0.028$. The accurate temperature was measured prior to the assay with an external thermometer (HI 935005N K-Thermocouple thermometer from HANNA).

Determination of T_{opt} can be done by fitting the peak of the curve to a third-degree polynomial trendline, differentiating the equation from the trendline and calculating its roots to find the highest value on the X-axis using equation 6. For the calculations of activity, the average of 3 measurements was used for each temperature and 3 – 4 sets of measurements were done for each enzyme.

$$X = \frac{-B \pm \sqrt{B^2 - 4AC}}{2A} \qquad (Eq. 6)$$

2.5 Rate of thermal inactivation ($T_{50\%}$)

$T_{50\%}$ of $VPR_{\Delta C}$ and $VPR_{\Delta C}$_W6Y was determined by monitoring the rate of thermal inactivation at selected temperatures and selected concentrations of $CaCl_2$. The samples were dialyzed in 25 mM Tris-Cl and 0-30 mM $CaCl_2$ overnight at 4 °C. Prior to heat denaturation stocks of 4 M NaCl and 100 mM EDTA were made and added to the sample to give the final concentrations of 25 mM Tris-Cl, 0 – 30 mM $CaCl_2$, 100 mM NaCl and 1 mM EDTA with a pH 8.95.

Samples were adjusted to approximately 1 U/mL depending on the availability of the enzyme and its stability at low calcium concentrations, they were then incubated in a water bath at a constant temperature and the activity measured at regular intervals at room temperature using a Cary50 Bio UV-Visible spectrometer (Varian). To calculate the rate of thermal inactivation at each temperature the data was fitted to display a decrease in velocity over time,

$$V = V_0 \cdot e^{-kt} \qquad (Eq.7)$$

V being the velocity (enzyme activity) measured at a given time, V_0 is the initial velocity, k is a first order rate constant given in s^{-1} and t being the time in seconds. For data fitting the temperature of the data set is plotted on the X-axis as 1/(K x 1000) and the natural logarithm of the rate constant k is plotted on the Y-axis to fit a linearized version of the Arrhenius equation. In equation 8, A stands for a pre-exponential factor, E_a is the activation energy, R is the universal gas constant in Joules/mol•K, and T is the temperature in Kelvin.

$$\ln(k) = 1000 \cdot \left(-\frac{E_a}{R \cdot T}\right) \cdot \ln(A) \qquad (Eq.8)$$

$T_{50\%}$ is defined as the temperature where 50% of the initial activity has been lost over 30 minutes. Calculating $T_{50\%}$ is dependent on its rate constant which is described by the equation:

$$k_{50\%}(s^{-1}) = \frac{\ln(100) - \ln(50)}{30\ min \cdot \frac{60\ sec}{min}} \qquad (Eq.9)$$

Therefore, $T_{50\%}$ can be written as:

$$T_{50\%} = \ln(k_{50\%}) - \left(\frac{\ln(A)}{E_a \cdot R^{-1}}\right) \qquad (Eq.10)$$

For each data set, five points were measured for an Arrhenius plot and the resulting $T_{50\%}$ value for corresponding sets was expressed as a mean a value with a standard deviation to estimate the uncertainty of measurements.

3 Results

3.1 Purification

Expression of $VPR_{\Delta C}$_N3P/I5P in cultures was done by the co-instructor K. R. Óskarsson and purification of $VPR_{\Delta C}$_N3P/I5P was done by the student. The purification was successful without significant loss in yield since expected yield is in the range of 40-60 %. SDS-PAGE results showed successful purification of the product. A single band was seen after the TETA column at approx 40 kDa, the same was seen for the Phe-Sepharose column (*Table 1*).

Table 1. The purification table for $VPR_{\Delta C}$_N3P/I5P.

Step	Volume [mL]	Conc. (c) [mg/mL]	Activity [U/mL]	Total activity units (AU) [U]	Total protein [mg]	Specific activity [U/mg]	Yield (%)	Purification (x)
Lysate Spin	48	4.4	5.1	242.8	209.2	1.2	100	1.0
(NH4)SO2 precipitate	60	4.6	5.7	343.3	275.0	1.2	140	1.1
TETA column	88	1.1	3.0	267.1	95.4	2.8	110	2.4
Phenyl speharose column	18	0.1	7.6	136.4	1.2	118.4	56	102

3.2 Optimal temperature assay (T_{opt})

The optimal temperature assay of $VPR_{\Delta C}$ and its variants may give information regarding the role of certain amino acid residues in thermal adaptation of the enzyme. The rise in activity in temperature. At the top is the peak of activity and the right side of the curve at higher temperatures is the area where thermal denaturation becomes significant within the timeframe of the activity measurements. At each temperature, the activity of the enzyme was assayed 3 times and the average used to calculate the specific activity (U/mg). To obtain reliable data each enzyme was assayed in 3 - 4 sets.

The curve that displays the optimal temperature for $VPR_{\Delta C}$ in *figure 10*, shows a steady increase in activity up until 55 °C where it reaches the peak of its activity and at 64 ± 0.1 °C the graph shows maximum activity, but as displayed with the error bars that is most likely due to noise and operator errors there for the calculated value is more accurate than the observed. The calculated value from fitting the peak of T_{opt} was 61.8 ± 0.8 °C. At temperatures above 64 °C, the activity decreased steadily due to fast heat denaturation of the enzyme. This is seen in *figure 10*, where relative specific activity is compared to the temperature of the buffer it was assayed in.

The increase in activity is relative to the increase in flexibility of the enzyme along with the enhanced rate of the reaction due to an increase in temperature. Since the enzyme is relatively stable at high concentrations of calcium, autoproteolysis is most likely not a large factor in these measurements.

Table 2. Polynomial equations were used to fit the peak of each T_{opt} curve to calculate T_{opt}. For VPRΔC data points 40-75 °C were used to obtain the fit, for $VPR_{\Delta C}$_N3P/I5P points 40-75 °C were also used and for VPR_W6Y data points from 25-70°C were used. The range of data points was determined by max R^2 value. The error for calculated values is based on the accuracy of the R^2 value.

Enzyme	R^2 Value	Observed T_{opt} (°C)	Calculated T_{opt} (°C)
$VPR_{\Delta C}$	0.99	64.1 ± 0.1	61.8 ± 0.8
$VPR_{\Delta C}$_N3P/I5P	0.98	63.2 ± 0.1	60.4 ± 1.2
$VPR_{\Delta C}$_W6Y	0.97	56.1 ± 0.1	54.6 ± 1.7

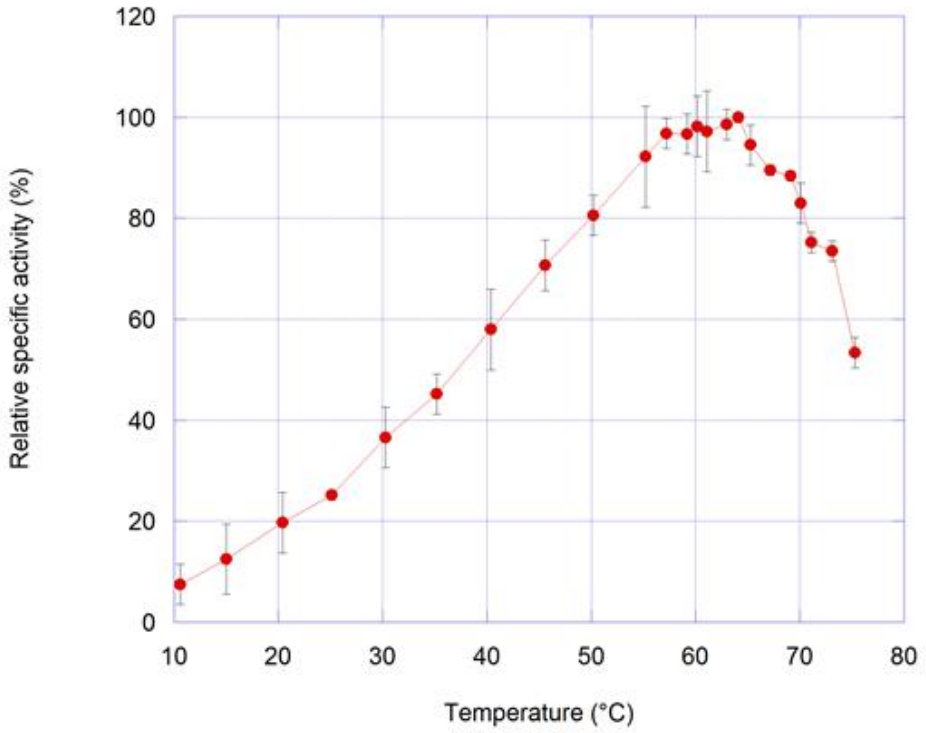

Figure 10. Relative activity of $VPR_{\Delta C}$ at selected temperatures between 10-75 °C. The enzyme was assayed for 30 seconds against 0.5 mM sAAPF-p-NA, in a buffer containing 25 mM Tris, pH 8.0, 10 mM $CaCl_2$.

Figure 11 shows the optimal temperature of $VPR_{\Delta C}$_N3P/I5P is similar to that of $VPR_{\Delta C}$, the observed value was 63.2 ± 0.1 °C and from calculating the value from the best fit T_{opt} is close to 60.4 ± 1.2 °C. The results are hard to interpret since the increase in stability against denaturation by heating as determined previously for this variant [34] is not observed in these measurements, resulting in no significant change in T_{opt} for the variant as compared to $VPR_{\Delta C}$.

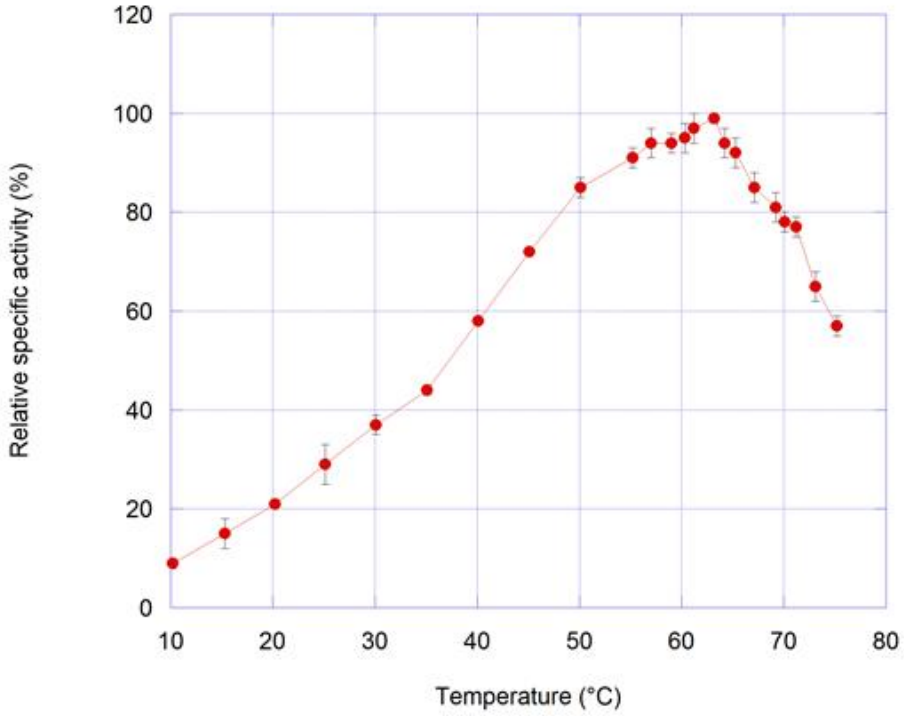

Figure 11. Relative activity of $VPR_{\Delta C}$_N3P/I5P at selected temperatures between 10-75 °C. The enzyme was assayed for 30 seconds against 0.5 mM sAAPF-p-NA, in a buffer containing 25 mM Tris, pH 8.0, 10 mM $CaCl_2$.

Figure 12 shows the curve for the optimal temperature of $VPR_{\Delta C}$_W6Y. The observed T_{opt} for the variant was 56.1 ± 0.1 °C, that is considerably lower than that of the $VPR_{\Delta C}$ and the calculated value for VPR_W6Y was 54.6 ± 1.7 °C. The lower T_{opt} observed reflects a lower thermal stability of this variant. The origin of this decrease in thermal stability is not known at present, however, but previous results have indicated the importance of the N-terminal region in the structural stability and activity of $VPR_{\Delta C}$.

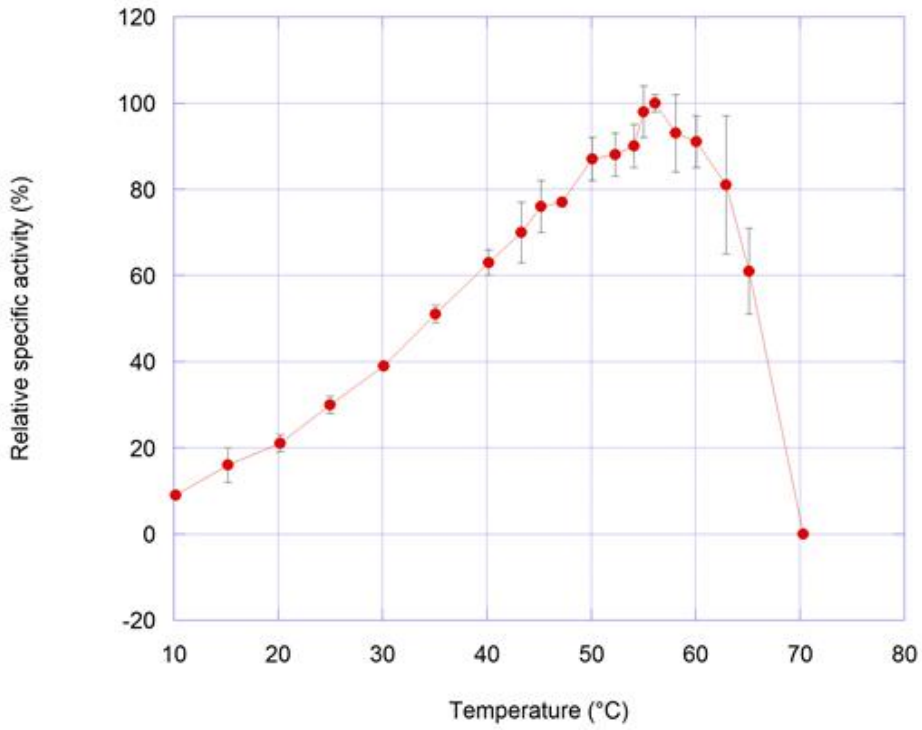

Figure 12. Relative activity of $VPR_{\Delta C}$_W6Y at selected temperatures between 10-70 °C. The enzyme was assayed for 30 seconds against 0.5 mM sAAPF-p-NA, in a buffer containing 25 mM Tris, pH 8.0, 10 mM $CaCl_2$.

Figure 13 shows the relative specific activity for $VPR_{\Delta C}$ and its variants over the temperature range of 10-75 °C. The results show two features most notable for further analysis. First, there seems to be no difference in T_{opt} for $VPR_{\Delta C}$ and $VPR_{\Delta C}$_N3P/I5P from these measurements. The cause of this is unknown at the moment. The second feature to be seen is the lowered T_{opt} of $VPR_{\Delta C}$_W6Y and its rapid denaturation above 60 °C. The location and the size of side chain could reduce the affinity of $VPR_{\Delta C}$_W6Y for calcium ions.

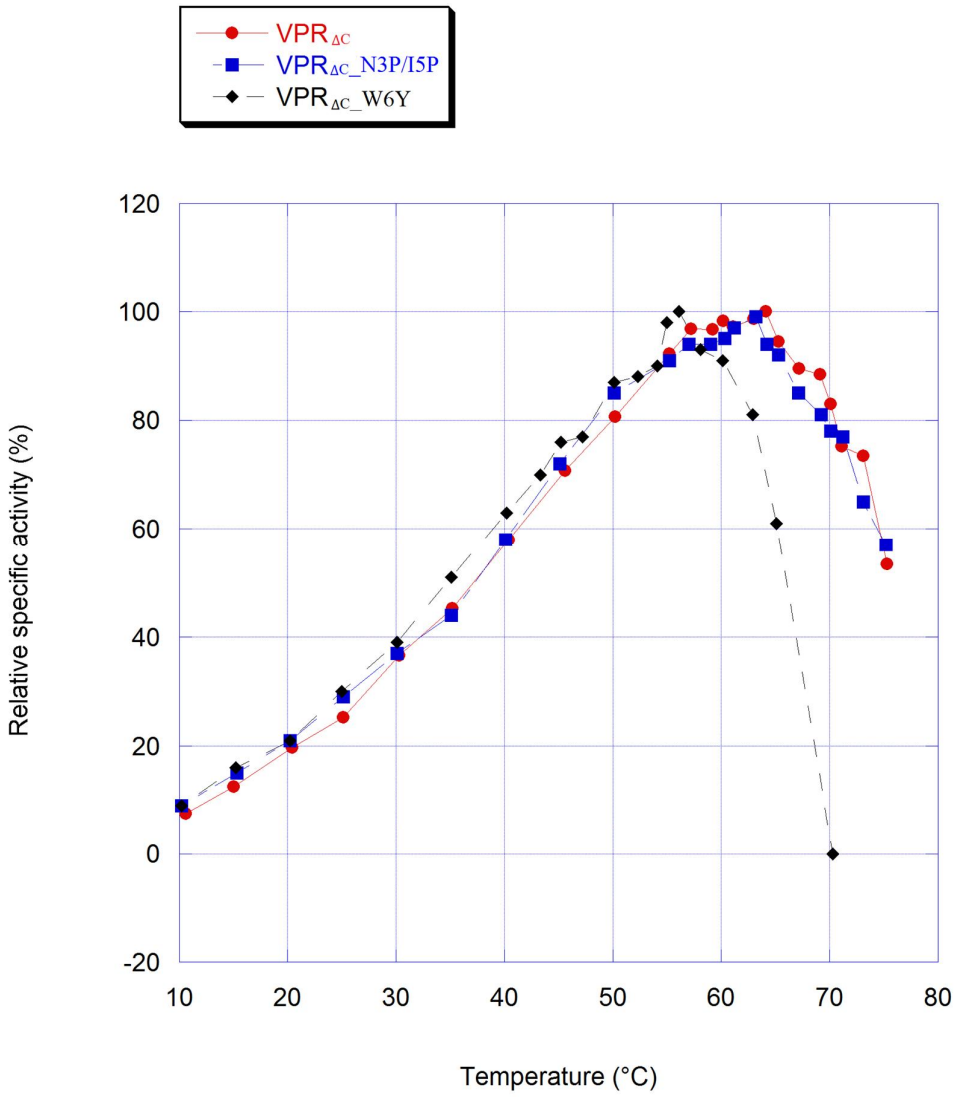

Figure 13. Comparison of relative activities of $VPR_{\Delta C}$ and its variants at selected temperatures between 10-75 °C. The enzymes were assayed for 30 seconds against 0.5 mM sAAPFN-p-NA, in a buffer containing 25 mM Tris, pH 8.0, 10 mM $CaCl_2$. The figure shows that there is little difference between $VPR_{\Delta C}$_N3P/I5P and $VPR_{\Delta C}$ but $VPR_{\Delta C}$_W6Y has shifted towards colder temperatures than $VPR_{\Delta C}$.

In *figure 14* are shown the specific activities of the enzymes. As can be seen, there is clearly a difference in terms of the specific activities for $VPR_{\Delta C}$ (red) and the two variants. $VPR_{\Delta C}$_N3P/I5P (blue) shows the lowest specific activity of the three enzymes. This double proline mutation has caused an increase in stability but this data and lowered k_{cat} could indicate increased rigidity in the enzyme structure which, however, is not realized in higher T_{opt} of the enzyme as was hypothesized for this study. Instead of shifting the T_{opt} to higher temperatures the $VPR_{\Delta C}$_N3P/I5P variant is a less efficient enzyme over the measured temperature range.

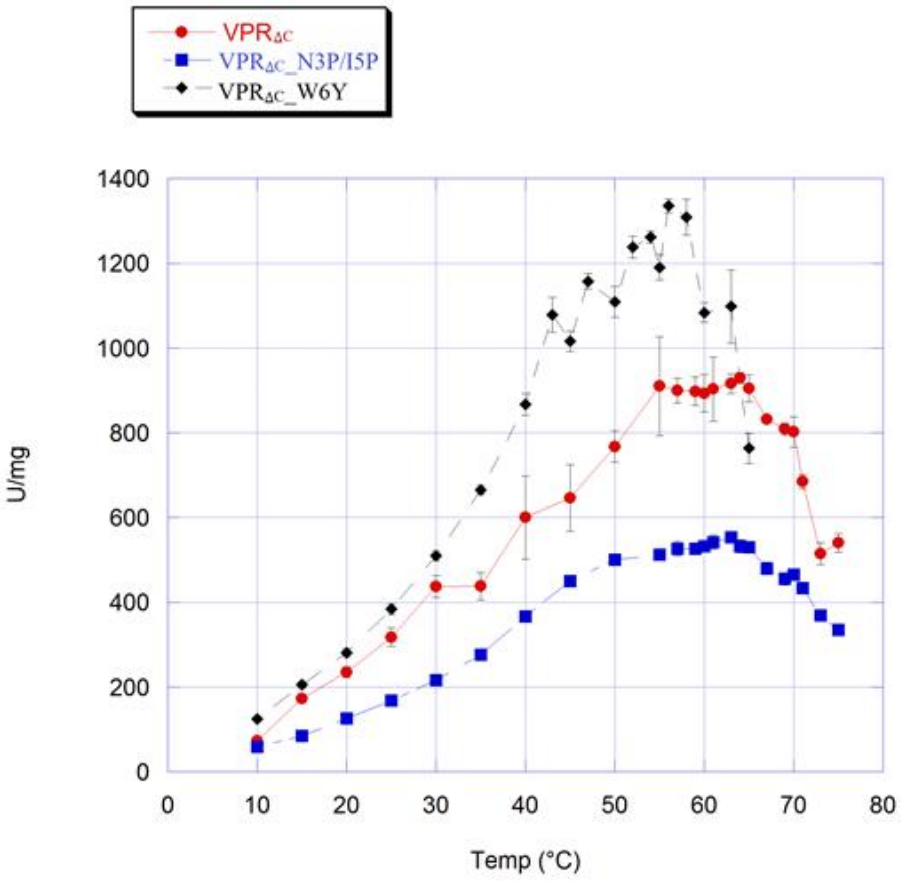

Figure 14. Comparison of specific activities for $VPR_{\Delta C}$ and its variants at selected temperatures between 10-75 °C. The enzymes were assayed for 30 seconds against 0.5 mM sAAPF-p-NA, in a buffer containing 25 mM Tris, pH 8.0, 10 mM $CaCl_2$. The figure shows the difference in specific activity of the enzymes at different temperatures. $VPR_{\Delta C}$ is shown in red (circles), $VPR_{\Delta C}$_N3P/I5P is shown in blue (boxes) and $VPR_{\Delta C}$_W6Y is shown in black (diamonds).

$VPR_{\Delta C}$_W6Y, on the other hand, has a higher specific activity than $VPR_{\Delta C}$ and has an exponential growth in activity until it reaches about 55 °C and after which the activity decreases. The top of the curve shows error mainly caused by the operator. The increase in specific activity could indicate increased flexibility of the enzyme but it has not been confirmed yet.

From *figure 15* we can approximate that there is an apparent change in the activation energy of the variants of $VPR_{\Delta C}$, but how much the change is or the accurate values are not available in this thesis. But however this supports the speculation in the aim of the project that the mutations have affected the adaption.

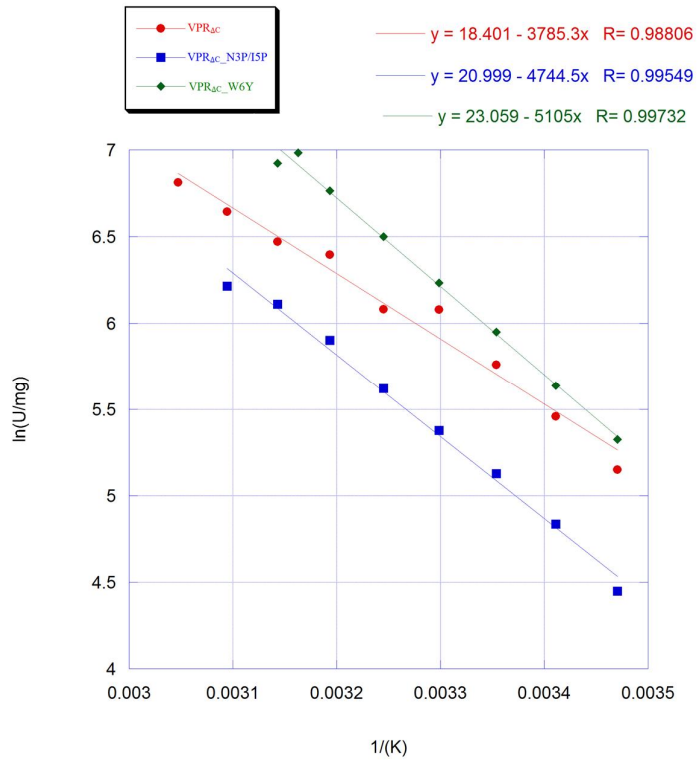

Figure 15. An Arrhenius plot of ln(U/mg) vs 1/K estimate, in order to see the apparent change in energy of activation and $\Delta H^{\#}$ for each enzyme. The slopes of the variants are steeper than that of $VPR_{\Delta C}$.

3.3 Rate of thermal inactivation ($T_{50\%}$) for $VPR_{\Delta C}$ and $VPR_{\Delta C}$_W6Y

For the rate of thermal inactivation both $VPR_{\Delta C}$ and $VPR_{\Delta C}$_W6Y were assayed at selected concentrations of $CaCl_2$ to see if the decreased thermal stability of the W6Y variant was a result of a diminished ability of the enzyme to bind Ca^{2+} at the proximal Ca-3 calcium binding site. The results in *figures 16 and 17* display a significant effect of calcium on thermal stability against thermal denaturation for both enzymes. The results confirm the lower thermal stability of the W6Y variant relative to that of $VPR_{\Delta C}$. There were also indications to suggest that the variant may also have a weaker calcium binding site than the original $VPR_{\Delta C}$. This can be seen for the results at 0 and 1 mM $CaCl_2$ concentrations, where the_variant does not show a significant increase in $T_{50\%}$ as $VPR_{\Delta C}$. In the absence or at 1 mM concentration of added $CaCl_2$ and in the presence of 1 mM EDTA, the effective concentration of Ca^{2+} should be below 1 mM and EDTA could bind calcium at a faster rate than the Ca3 binding site. At these low concentrations, $VPR_{\Delta C}$ shows an improvement in $T_{50\%}$ by 2.6 °C, but $VPR_{\Delta C}$_W6Y shows only 0.4 °C increase in $T_{50\%}$. This lag region could indicate that $VPR_{\Delta C}$_W6Y has a lower calcium binding affinity than the wild type, which may be because the Ca3 binding site has a lower affinity for Ca^{2+} as EDTA appears to compete more with its binding.

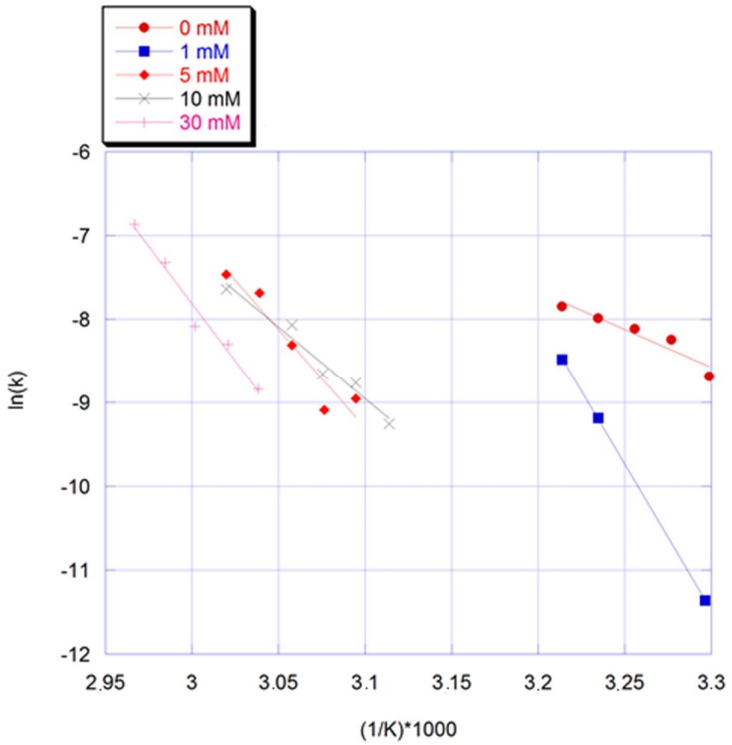

Figure 16. Arrhenius plot for $VPR_{\Delta C}$ at selected concentrations of $CaCl_2$. Samples without calcium (0 mM) is displayed as red circles, 1 mM $CaCl_2$ is shown as blue boxes, 5 mM. is shown as red diamonds, 10 mM is shown as a gray X and 30 mM is shown as a pink +. ln(k) is the natural logarithm of the first-order rate k (s^{-1}), constant for thermal inactivation at each temperature

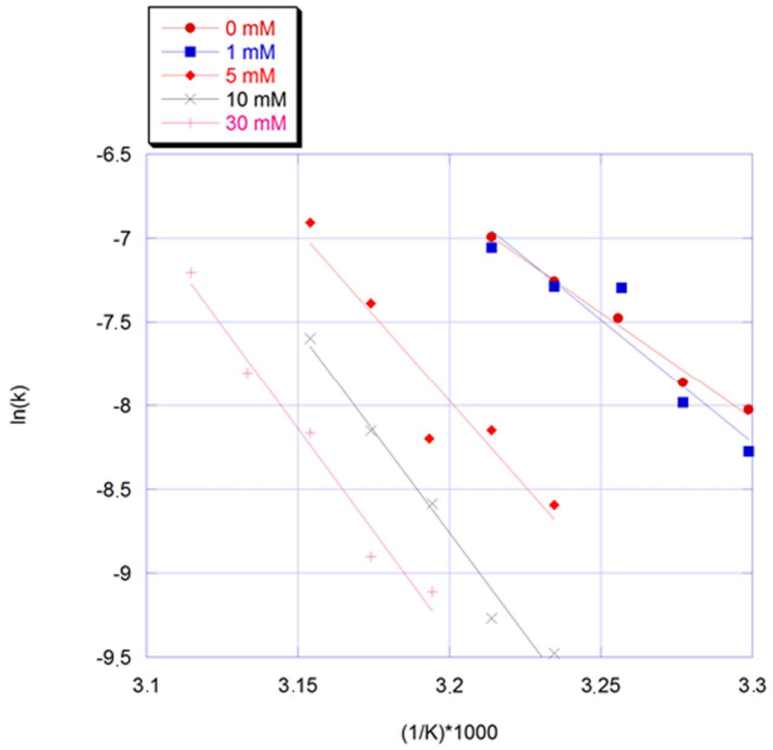

Figure 17. Arrhenius plot for $VPR_{\Delta C}$_W6Y at selected concentrations of $CaCl_2$. 0 mM conc. is shown as red circles, 1 mM conc. is shown as blue squares, 5 mM conc. is shown as red diamonds, 10 mM conc. is shown as a gray X and 30 mM concentration is shown as a pink +. ln(k) is the natural logarithm of the rate constant k (s^{-1}).

Table 3 shows the tabular data calculated according to equation 10 from the data used in *figures 16 and 17.* At the lowest concentrations of calcium, other factors may affect the rate of thermal inactivation, such as autoproteolysis, since subtilisin-like serine proteases are very dependent on calcium for stabilization and proteases are prone to autoproteolysis [1].

Table 3. Thermal stability of $VPR_{\Delta C}$ and $VPR_{\Delta C}$_W6Y as a function of $CaCl_2$ concentration. The samples were incubated in 25 mM Tris-Cl, 0 – 30 mM $CaCl_2$, 100 mM NaCl and 1 mM EDTA with a pH 8.95 for the appropriate amount of time, then assayed against 0.5 mM sAAPF-p-NA in 100 mM Tris, pH 8.6, 10 mM $CaCl_2$ for remaining activity. $T_{50\%}$ the temperature at which half the enzyme activity was lost in 30 min. was determined from the Arrhenius plots (see Material and methods for details).

$CaCl_2$ (mM)	**$VPR_{\Delta C}$ $T_{50\%}$**	**VPR_W6Y $T_{50\%}$**
0	37.1 ± 0.1	31.7 ± 0.3
1	39.7 ± 0.02 [2)]	32.1 ± 0.05
5	53.9 ± 0.09	39.8 ± 0.06
10	56.2 ± 0.002	42.7 ± 0.3
15[1)]	56.4 ± 0.1	43.6 ± 0.3
30	60.4 ± 0.4	44.5 ± 0.9

1) The numeric value for $VPR_{\Delta C}$ and for $VPR_{\Delta C}$_W6Y at 15 mM $CaCl_2$ are from Óskarsson K. R. [8, unpublished data].

2) At 1 mM for $VPR_{\Delta C}$, only three data points were used for the Arrhenius plot and thus has a high uncertainty.

Figure 18 compares the $T_{50\%}$ values from table 3. From the data, it may be that the mutation has reduced the thermal stability of the enzyme by possibly lowering the affinity of the Ca3 binding site in $VPR_{\Delta C}$_W6Y. The strongest evidence for this claim is seen in the $T_{50\%}$ value between 0 and 1 mM concentration for $VPR_{\Delta C}$_W6Y, where there seems to be no significant increase in $T_{50\%}$.

The data from this thesis may indicate that the effect of the mutation W6Y has a negative impact on the Ca3 binding site due to its location on the N-terminus resulting in lowered thermal stability, although it is not impossible that the mutation has also affected the total structure of the enzyme causing a reduced affinity for calcium at the other binding sites as well.

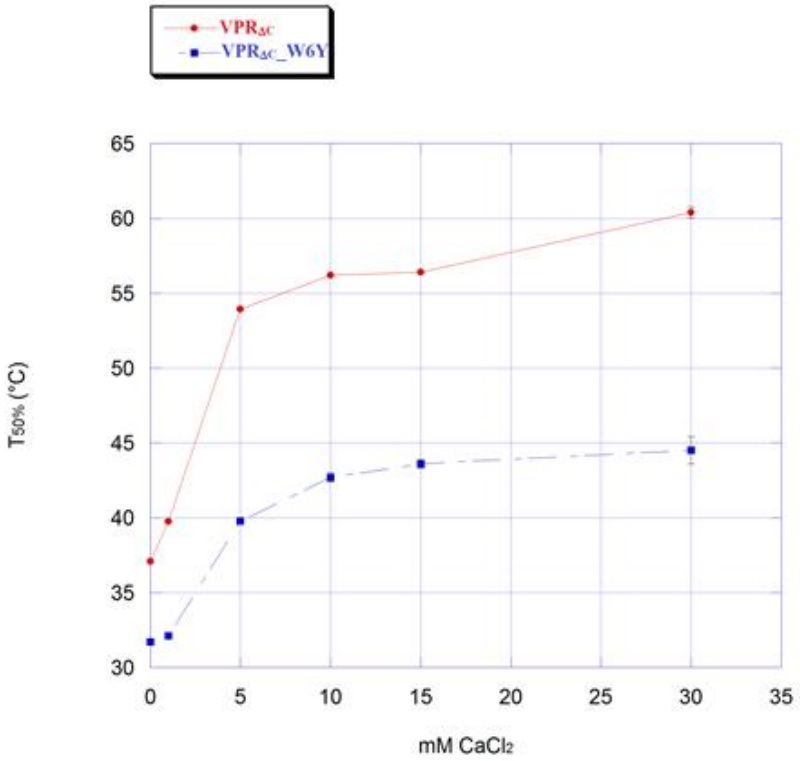

Figure 18. The comparison of $T_{50\%}$ values for $VPR_{\Delta C}$ (red) and $VPR_{\Delta C}$_W6Y (blue) displayed against the concentration of calcium in the incubation solution. Values were obtained from the rate constant k according to equation 10 and taken from Table 3.

4 Conclusions

For subtilisin-like proteases calcium plays a crucial role in stability, it is suggested that the enzymes are at an equilibrium between structurally similar but energetically distinct states: N and N*. This equilibrium can be altered by point mutations or by calcium binding. According to that model, mutations that only stabilize in the precense of calcium, stabilize the N state relative to N*. In this model the N* state has a much faster rate of inactivation than N, therefor all mutations that shift the equilibrium from N* to the N state could increase stability for the enzyme [40].

In the case of $VPR_{\Delta C}$_N3P/I5P, there was no shift in T_{opt} observed even though it has a higher T_m and $T_{50\%}$ than $VPR_{\Delta C}$. This result is unexpected as this variant had shown an increase in thermal stability in previous experimentation [8,34]. The data regarding the energy of activation is only apparent datum. It is not conclusive on the effects of the mutations on the energy of activation. However, they give us an idea of what has happened to the enzyme, the mutations were selected from a thermophilic enzyme and thus, they should increase the enthalpy of activation and apparently they do. As seen in equation 2 on page 4, the classical Gibbs-Helmholtz relation, the activity of psychrophilic enzymes is dependent on lowering the free energy of activation $\Delta G^{\#}$. One strategy that has been suggested is that evolutionary pressure has led to an increase in Km for the enzyme. According to the transition state theory when an enzyme encounters its substrate, the enzyme-substrate complex falls into an energy pit. By increasing the K_m the pit isn't as deep making it easier for the enzyme to overcome the energy barrier thus increasing its activity [12].

For $VPR_{\Delta C}$_W6Y, the results were more revealing. There was a noticeable change in T_{opt} of about 8 °C for the observed value from measurements but 7.2 °C for the calculated value, as compared to the truncated enzyme. There was also a significant drop in $T_{50\%}$ for the enzyme, at 15 mM $CaCl_2$ where the difference was 12.8 °C. The decrease in thermal stability could be mainly due to reduced affinity for calcium at Ca3 binding site due to the proximity of the mutation site. This is seen in the difference between 0 mM – 1 mM, where there is no significant increase in $T_{50\%}$, which could indicate that the binding affinity of $VPR_{\Delta C}$_W6Y at the Ca3 binding site is less or equal to the affinity EDTA has for calcium ions. Thus, as can be observed from *figure 18,* the W6Y variation significantly lowers the thermal stability of $VPR_{\Delta C}$ and that it may be partly explained by lowered calcium binding affinity. Further studies are required however to elucidate that point. To study the binding affinity of the Ca3 binding site, the protein binding energetics could be studied using isothermal titration calorimetry [39].

From our preliminary data on the energy of activation, it seemed that $VPR_{\Delta C}$_W6Y had a higher energy of activation than $VPR_{\Delta C}$. These results were the opposite of what was expected since the T_{opt} and thermal stability is lower for $VPR_{\Delta C}$_W6Y [Kristjánsson M. M. unpublished data].

5. References

1. Kristjánsson, M. M. (2012). Thermostable subtilases (Subtilisin-like serine proteinases). *Thermostable Proteins: Struct Stab* Des, 67-97.

2. Miyazaki, K. & Arnold, F. H. (1999). Exploring nonnatural evolutionary pathways by saturation mutagenesis: rapid improvement of protein function. *J Mol Evol* **49**(6), 716-720.

3. Zhao, H., Giver, L., Shao, Z., Affholter, J. A. & Arnold, F. H. (1998). Molecular evolution by staggered extension process in vitro recombination. *Nat Biotechnol.* **16**(258), 258 - 261.

4. Miyazaki, K., Wintrode, P. L., Grayling, R. A., Rubingh, D. N. & Arnold, F. H. (2000). Directed evolution study of temperature adaption in a psychrotrophic enzyme. *J Mol Biol.* **297**(4), 1015-1026.

5. Arnórsdóttir, J., Kristjánsson, M. M. & Ficner, R. (2005). Crystal structure of a subtilisin-like serine proteinase from a psychrotrophic Vibrio species reveals structural aspects of cold adaption. *FEBS J.* **272**, 832-845.

6. Sigurðardóttir, A. G., Arnórsdóttir, J., Thorbjarnardóttir, S. H., Eggertsson, G. Suhre, K. & Kristjánsson M. M. (2009). Characteristics of variants designed to incorporate a new ion pair into the structure of a cold adapted subtilisin-like serine proteinase. *BBA*. **1794**, 512-518.

7. Arnórsdóttir, J., Helgadóttir, S., Thorbjarnardóttir, S. H., Eggertssson, G. & Kristjánsson M. M. (2007). Effects of selected Ser/Ala and Xaa/Pro mutations on the stability and catalytic properties of a cold adapted subtilisin-like serine proteinase. *BBA*. **1774**, 749-755.

8. Óskarsson, K. R. (2015). Rational design of the cold-active subtilisin-like serine protease VPR towards higher activity and thermostability.(Master‘s Thesis). The university of Iceland. Available from Skemman. URL:http://hdl.handle.net/1946/21648

9. Lam S. Y., Yeung R. C. Y., Yu TH., Sze, KH. & Wong, KB (2011). A Rigidifying Salt-Bridge Favors the Activity of Thermophilic Enzyme at High Temperatures at the Expense of Low-Temperature Activity. *PLoS Biol*. **9**(3), e1001027.

10. Arnold, F. H., Wintrode, P. L., Miyazaki, K. & Gershenson, A. (2001). How enzymes adapt: lessons from directed evolution. *Trends Biochem Sci* **26**(2), 100-106.

11. Fields, P. A., Dong, Y., Meng, X. & Somero, G. N. (2015). Adaptations of protein structure and function to temperature: there is more than one way to skin a cat. *The J Exp Biol* **218**, 1801-1811.

12. Feller., G. (2013). Psychrophilic Enzymes: From folding to function and biotechnology. *Scientifica* **2013**. 1-28.

13. Rodrigues, D. F. & Tiedje, J. M (2008). Coping with Our Cold Planet. *Appl Environ Microbiol.***74**(6),1677-86.

14. D'Amico, S., Marx, JC., Gerday, C. & Feller, G (2002). Activity-Stability Relationships in Extremophilic Enzymes. *J Biol Chem*. **278**(10), 7891-7896.

15. Collins, T., Meuwis, MA., Gerday, C. & Feller, G (2003). Activity, Stability and Flexibility in Glycosidases Adapted to Extreme Thermal Environments. *J Mol Biol.* **328**(2), 419-428.

16. Di Cera, E. (2009). Serine proteases, *IUBMB life*. **61**, 510-515.

17. Polgár, L. (2005). The catalytic triad of serine peptidases. *Cell Mol Life Sci.* **62**, 2161-2172.

18. Hedstrom, L. (2002). Serine protease mechanism and specificity. *Chem Rev* **202**, 4501-4523.

19. Page, M. J. & Di Cera, E. (2008). Serine peptidases: Classification, structure and function. *Cell Mol Life Sci*. **65**, 1220-1236.

20. Siezen, R. J. & Leunissen, J. A. (1997). Subtilases: the superfamily of subtilisin-like serine proteases. Protein Sci **6**, 501-523.

21. Rawlings, N.D., Waller, M., Barrett, A. J. & Bateman, A. (2014). MEROPS: the database of proteolytic enzymes, their substrates, and inhibitors. *Nucleic Acids Res.* **42**, D503-D509.

22. Marie-Claire C., Yabuta Y., Suefuji K., Matsuzawa, H. & Shinde, U. (2001). Folding pathway mediated by an intramolecular chaperone: The structural and functional characterization of the aqualysin I propeptide. *J Mol Biol.* **305,** 151-161

23. Bryan, P., Wang, L., Hoskins, J., Ruvinov, S., Strausberg, S., Alexander, P., Almog, O., Gilliland, G. & Gallagher, T. (1995). Catalysis of a protein folding reaction: Mechanistic implication of the 2.0 Å structure of the subtilisin-prodomain complex. *Biochem* **26**, 10310-10318.

24. Bryan, P. N. (2002). Prodomains and protein folding catalysis. *Chem Rev* **120**, 4805-4815.

25. Strausberg, S. L., Alexander, P., Wang, L., Schwarz, F. & Bryan, P.,(1993). Catalysis of a protein folding reaction: Thermodynamic and kinetic analysis of subtilisin BPN' interactions with its propeptide fragment. *Biochem*. **32**, 8112-8119.

26. Kristjánsson, M. M., Magnússon, Ó.T., Guðmundsson, H. M., Alfreðsson, G. Á., Matsuzawa, H. (1999*).* Properties of a subtilisin-like proteinase from a psychrotrophic Vibrio species. *Eur. J. Biochem*. **260**, 752-760.

27. Loladze, V. V., Ibarra-Molero, B., Sanchez-Ruiz, J, M. & Makhatadze, G. I. (1999). Engineering a thermostable protein via optimization of charge-charge interactions on the protein surface*. Biochem*. **38**, 16419-16423.

28. Serrano, L., Sancho, J., Hirshberg, M. & Fersht, A. R. (1992). *Alpha-helix stability in proteins. I*. Empirical correlations concerning substitutions of side-chains at the N and C-caps and the replacement of alanine by glycine or serine at solvent-exposed surfaces. *J Mol Biol*. **227**, 544-559

29. Perry, L. J. & Wetzel, R. (1984). Disulfide bond engineered into T4 lysozyme: stabilization of the protein toward thermal inactivation. *Science* **226**, 555-557.

30. Ishikawa, Nakamura, H., Morikawa, K. & Kanaya, S. (1993). Stabilization Escherichia coli ribonuclease HI by cavity-filling mutations withing a hydrophobic core. *Biochem*. **32**, 6171-8.

31. Ayuso-T., S., Abioan, O. & Sancho, J. (2011). Underexposed polar residues and protein stabilization. *Protein Eng Des Sel* **24**,171-177.

32. Arnórsóttir J., Smáradóttir R. B, Magnússon, Ó. T., Thorbjarnardóttir, S. H., Eggertsson G., Kristjánsson M. M. (2002). Characterization of a cloned subtilisin-like serine proteinase from a psychrotrophic Vibrio species. *Eur. J. Biochem*. **269**, 5536-5546.

33. Wigley, D. B., Clarke, A. R., Dunn, C. R., Barstow, D. A., Atkinson, T., Chia, W. N., Muirhead, H. & Holbrook, J. J. (1987). The engineering of a more thermally stable lactate dehydrogenase by reduction of the area of water-accessible hydrophobic surface. BBA **916**, 145-148.

34. Arnórsdóttir, J., Sigtryggsdóttir, Á. R., Thorbjarnardóttir, S. H. & Kristjánsson, M. M. (2009). Effect of Proline Substitutions on Stability and Kinetic Properties of a Cold-Adapted Subtilase. *J Biochem.* **145**(3), 325-329.

35. Zaman, Z. & Verwilghen, R. L. (1979). Quantitation of proteins solubilized in sodium dodecyl sulfate-mercaptoethanol-tris electrophoresis buffer. *Anal Biochem*. **100**, 64-69

36. Schägger, H. & von Jagow, G. (1987) Tricine-sodium dodecyl sulfate-polyacrylamide gel electrophoresis for the separation of proteins in the range of 1 to 100 kDa. *Anal Biochem*. **166**(2), 368-379.

37. Candiano, G., Bruschi, M., Musante, L., Ghiggeri, GM., Orecchia, P. & Righetti, PG. (2004). Blue silver: a very sensitive colloidal Coomassie G-250 staining for proteome analysis. *Electrophoresis* **25**(9), 1327-1333.

38. Pettersen, E. F., Goddard, T. D., Huang, C. C., Couch, G. S., Greenblatt, D. M., Meng E. C. & Ferrin, T. E. (2004). UCSF Chimera a visualization system for exploratory research and analysis. *J Comput Chem*. **25**(13), 1605-1612.

39. Leavitt, S. & Freire, E. (2001). Direct measurement of protein binding energetics by isothermal titration calorimetry, *Curr Opin Struct Biol.* **11**(5), 560-566.

40. Alexander, P. A., Ruan, B., Strausberg, S. L. & Bryan P. N. (2001). Stabilizing mutations and calcium-dependent stability of subtilisin. *Biochem.* **40**(35), 10640-4.

5 Appendix A

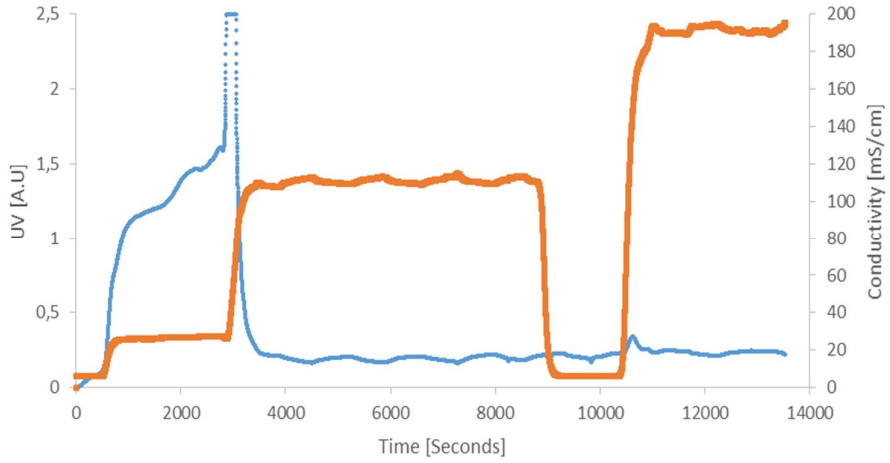

Figure 19. The purification of VPR$_{\Delta C}$_N3P/I5P on a Z-D-Phe-TETA sepharose column. The absorbance at 280 nm is shown in blue (Y-axis on the left) and the conductivity is shown in orange (Y-axis on the right). The column had been equilibrated with buffer A prior to loading. The first peak is after eluting non-specific binding proteins with buffer A + 0.5 M NaCl, then equilibrated again with buffer A, then finally bound proteins were eluted using buffer A + 2 M GdnCl. Fractions were collected into sample tubes with 2 mL of 2 M AMSO. Activity was found in the last peak, seen after seconds 10000 on the blue line.

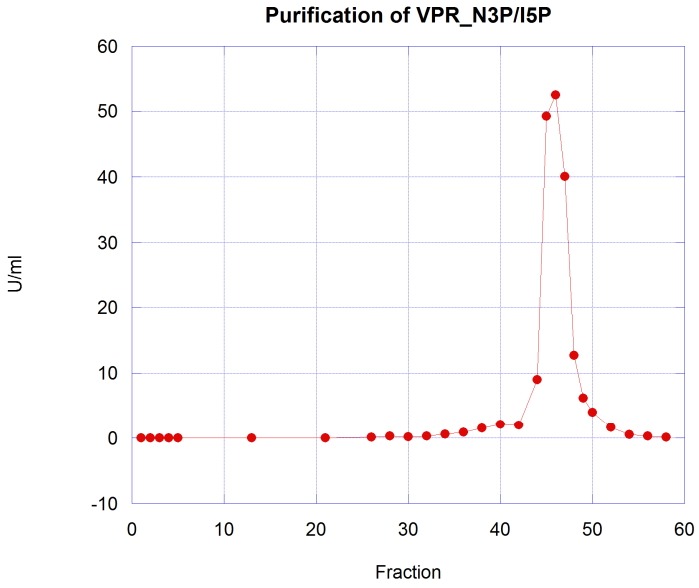

Figure 20. Condensing step for VPR$_{\Delta C}$_N3P/I5 purification. The activity of fractions was used to determine the purification curve, the A_{280} data was unreliable and therefore not used.

Appendix B

Appendix B contains datasets from T_{opt} assays, for the data set of $VPR_{\Delta C}$ the first set could not be used due to differences in substrate concentration, the later data sets in figure 20 and 21 contain 4 lots of measurements. This was done to improve the fit of the curve by obtaining more data.

Control (°C)	Average °C L1	Average °C L2	Average °C L3	Uncertainty °C L1	Uncertainty °C L2	Uncertainty °C L3	Average Total (°C)	Uncertainty (°C)	Relative Average L1	Relative Average L2	Relative Average L3	Relative Uncertainty L1	Relative Uncertainty L2	Relative Uncertainty L3	Average Relative Total (U/mg)	Relative Uncertainty (U/mg)
10	10,6			0,1			10,6	0,1	0,0749			0,04			0,075	0,04
15	14,8	15,2		0,1	0,04		15,0	0,1	0,1319	0,1173		0,06	0,05		0,125	0,07
20	20,6	20,2		0,1	0,03		20,4	0,1	0,2183	0,1756		0,05	0,03		0,197	0,06
25	25,1	25,1		0,2	0,03		25,1	0,2	0,2604	0,2442		0,01	0,01		0,252	0,01
30	30,2	30,4		0,2	0,12		30,3	0,2	0,4012	0,3299		0,06	0,03		0,366	0,06
35	35,2			0,1			35,2	0,1	0,4515			0,04			0,452	0,04
40	40,4			0,2			40,4	0,2	0,5798			0,08			0,580	0,08
45	45,6			0,2			45,6	0,2	0,7073			0,05			0,707	0,05
50	50,3	50,2		0,0	0,10		50,2	0,1	0,7914	0,8204		0,03	0,03		0,806	0,04
55	55,4	55,2	55,2	0,2	0,06	0,10	55,2	0,2	0,9970	0,9238	0,9207	0,09	0,03	0,02	0,922	0,10
57			57,2			0,10	57,2	0,1			0,9683			0,03	0,968	0,03
59			59,2			0,09	59,2	0,1			0,9667			0,04	0,967	0,04
60	60,1	60,2	60,2	0,1	0,10	0,09	60,2	0,2	0,9183	1,0000	0,9638	0,05	0,03	0,01	0,982	0,06
61			61,1			0,07	61,1	0,1			0,9723			0,08	0,972	0,08
63			63,0			0,07	63,0	0,1			0,9861			0,03	0,986	0,03
64			64,1			0,07	64,1	0,1			1,0000			0,01	1,000	0,01
65	65,3	65,5	65,1	0,1	0,09	0,06	65,3	0,2	1,0000	0,9655	0,9242	0,03	0,03	0,01	0,945	0,04
67			67,2			0,10	67,2	0,1			0,8952			0,01	0,895	0,01
69			69,1			0,10	69,1	0,1			0,8838			0,01	0,884	0,01
70	70,1	70,1	70,2	0,1	0,02	0,1	70,1	0,1	0,9596	0,8885	0,7719	0,03	0,03	0,01	0,830	0,04
71			71,1			0,10	71,1	0,1			0,7522			0,02	0,752	0,02
73			73,1			0,10	73,1	0,1			0,7347			0,02	0,735	0,02
75	75,2	75,4	75,1	0,1	0,09	0,10	75,3	0,1	0,7771	0,5080	0,5601	0,03	0,01	0,01	0,534	0,03

Figure 21. The dataset from T_{opt} measurements of $VPR_{\Delta C}$

Control (°C)	Average °C L1	Average °C L2	Average °C L3	Average °C L4	Unc. °C L1	Unc. °C L2	Unc. °C L3	Unc. °C L4	Average total (°C)	Unc. °C	Relative Average L1	Relative Average L2	Relative Average L3	Relative Average L4	Relative Unc. L1	Relative Unc. L2	Relative Unc. L3	Relative Unc. L4	Average Relative Total (U/mg)	Relative Unc. (U/mg)
10	10,7			10,2	0,1	0,2		0,0	10,2	0,1	0,077			0,094	0,100			0,006	0,09	0,01
15	15,0	15,4		15,1	0,1	0,1		0,1	15,3	0,1	0,107	0,146		0,146	0,060	0,015		0,037	0,15	0,03
20	20,5	20,3		20,1	0,1	0,1		0,1	20,2	0,1	0,198	0,209		0,219	0,100	0,023		0,001	0,21	0,01
25	25,2	25,1		25,1	0,1	0,1		0,1	25,1	0,1	0,286	0,293		0,282	0,106	0,025		0,047	0,29	0,04
30	30,4	30,2		30,0	0,2	0,1		0,1	30,1	0,1	0,331	0,381		0,359	0,100	0,028		0,019	0,37	0,02
35	35,5			35,1	0,1	0,1		0,1	35,1	0,1	0,470			0,439	0,054			0,009	0,44	0,01
40	40,0			40,1	0,2			0,1	40,1	0,1	0,488			0,583	0,100			0,005	0,58	0,00
45	45,2			45,1	0,1			0,1	45,1	0,1	0,606			0,716	0,100			0,004	0,72	0,00
50	50,0	50,2		50,0	0,1			0,0	50,1	0,0	0,749	0,867		0,841	0,100	0,026		0,013	0,85	0,02
55	55,3	55,4	55,1	55,2	0,1		0,1	0,1	55,2	0,1	0,746	0,952	0,918	0,908	0,071	0,037	0,019	0,013	0,91	0,02
57			57,1	57,0			0,1	0,1	57,0	0,1			0,938	0,945			0,056	0,014	0,94	0,03
59			59,0	59,0			0,1	0,1	59,0	0,1			0,934	0,949			0,019	0,013	0,94	0,02
60	60,0	60,6	60,1	60,1	0,2	0,2	0,1	0,1	60,3	0,1	0,797	0,998	0,954	0,936	0,116	0,010	0,058	0,016	0,95	0,03
61			61,1	61,2			0,1	0,1	61,2	0,1			0,950	0,985			0,044	0,021	0,97	0,03
63		63,2	63,2			0,1	0,1		63,2	0,1		1,000	0,983			0,013	0,011	0,99	0,01	
64			64,2	64,2			0,1	0,1	64,2	0,1			0,888	1,000			0,045	0,018	0,94	0,03
65	65,2	65,4	65,2	65,2	0,2	0,1	0,1	0,1	65,3	0,1	0,905	1,000	0,857	0,993	0,100	0,007	0,058	0,012	0,92	0,03
67			67,1	67,1			0,1	0,1	67,1	0,1			0,827	0,882			0,053	0,015	0,85	0,03
69			69,3	69,1			0,1	0,0	69,2	0,1			0,758	0,860			0,042	0,026	0,81	0,03
70	70,1	70,1	70,1	70,2	0,1	0,1	0,1	0,1	70,1	0,1	1,000	0,953	0,748	0,812	0,128	0,038	0,011	0,021	0,78	0,02
71			71,2	71,1			0,1	0,1	71,2	0,1			0,711	0,828			0,013	0,026	0,77	0,02
73			73,2	73,0			0,1	0,1	73,1	0,1			0,613	0,696			0,034	0,020	0,65	0,03
75	75,3	75,5	75,1	75,2	0,2	0,1	0,1	0,1	75,2	0,1	0,791	0,646	0,506	0,644	0,100	0,011	0,015	0,030	0,57	0,02

Figure 22. The dataset from T_{opt} measurements of $VPR_{\Delta C}$_N3P/I5P

Control (°C)	Average °C L1	Average °C L2	Average °C L3	Average °C L4	Unc. °C L1	Unc. °C L2	Unc. °C L3	Unc. °C L4	Average total (°C)	Unc. °C	Relative Average L1	Relative Average L2	Relative Average L3	Relative Average L4	Relative Unc. L1	Relative Unc. L2	Relative Unc. L3	Relative Unc. L4	Average Relative Total (U/mg)	Relative Unc. (U/mg)
10	10,2	10,2		10,2	0,1	0,0		0,1	10,2	0,1	0,276	0,120		0,056	0,06	0,02		0,006	0,09	0,01
15	15,1	15,2		15,2	0,1	0,1		0,1	15,2	0,1	0,386	0,187		0,136	0,03	0,07		0,006	0,16	0,04
20	20,4	20,1		20,4	0,1	0,1		0,1	20,2	0,1	0,460	0,227		0,203	0,06	0,03		0,012	0,21	0,02
25	24,9	24,9		25,1	0,1	0,0		0,1	25,0	0,0	0,561	0,319		0,272	0,07	0,01		0,024	0,30	0,02
30	30,2	30,1		30,1	0,1	0,0		0,1	30,1	0,1	0,765	0,414		0,366	0,05	0,01		0,010	0,39	0,01
35	35,3	35,1		35,1	0,1	0,1		0,1	35,1	0,1	0,876	0,534		0,482	0,02	0,01		0,022	0,51	0,02
40	40,3	40,2	40,2	40,2	0,1	0,1	0,1	0,1	40,2	0,1	0,940	0,657	0,900	0,605	0,06	0,03	0,07	0,034	0,63	0,03
43			43,1	43,3			0,1	0,0	43,3	0,1			0,938	0,699			0,09	0,071	0,70	0,07
45	45,2	45,2	45,1	45,3	0,1	0,1	0,1	0,1	45,2	0,1	0,924	0,795	0,993	0,732	0,04	0,02	0,02	0,100	0,76	0,06
47			47,1	47,2			0,1	0,1	47,2	0,1			0,976	0,769			0,06	0,013	0,77	0,01
50	50,1	50,0	50,1	50,1	0,1	0,1	0,1	0,1	50,1	0,1	0,989	0,894	0,999	0,837	0,04	0,08	0,08	0,024	0,87	0,05
52			52,1	52,3			0,1	0,1	52,3	0,1			0,949	0,882			0,05	0,053	0,88	0,05
54			54,2	54,1			0,1	0,1	54,1	0,1			0,958	0,905			0,01	0,045	0,90	0,05
55	55,2	55,0	55,1	55,0	0,1	0,1	0,1	0,1	55,0	0,1	1,000	1,000	0,945	0,955	0,01	0,03	0,06	0,095	0,98	0,06
56			56,0	56,1			0,1	0,1	56,1	0,1			0,946	1,000			0,05	0,021	1,00	0,02
58			58,1	58,1			0,1	0,1	58,1	0,1			1,000	0,934			0,07	0,092	0,93	0,09
60	60,1	60,1	60,1	60,0	0,1	0,0	0,1	0,1	60,1	0,1	0,799	0,951	0,816	0,873	0,01	0,03	0,04	0,081	0,91	0,06
63			63,2	62,9			0,1	0,1	62,9	0,1			0,800	0,808			0,21	0,161	0,81	0,16
65	65,2	65,2	65,2	65,0	0,0	0,0	0,0	0,1	65,1	0,1	0,338	0,420	0,513	0,800	0,17	0,14	0,08	0,057	0,61	0,10
70	70,1	70,3			0,0	0,0			70,3		0,000	0,000			0,000	0,00			0,00	

Figure 23. The dataset from T_{opt} measurements for $VPR_{\Delta C}$_W6Y.